

D3.4

NEMMO Biomimetic and Multi-material Solutions

Lead Beneficiary	DCU
Delivery date	2021-06-03
Dissemination level	Public
Status	Public
Version	2.4
Keywords	Testing methodologies, Multi-material, Fatigue, Composite blades, biofouling, Ageing



This project has received funding from the European Union's Horizon 2020 research and innovation programme under grant agreement No 815278.

www.nemmo.eu  [@NEMMO_Project](https://twitter.com/NEMMO_Project)  info@nemmo.eu

Information

Grant Agreement Number	815278
Project Acronym	NEMMO
Work Package	3
Task(s)	3.1; 3.2; 3.3
Deliverable	D3.4
Title	Deliverable 3.4 NEMMO Biomimetic and Multi-material Solutions
Author(s)	Chloe Richards, Adrián Delgado Ollero, Célia Mercader, Asa Eitan, Yan Delauré, Fiona Regan, Dulce Muñoz, Cecilia Agustin, Gemma Berriozabal
File Name	NEMMO_D3.4_NEMMO_Biomimetic_and_Multi-material_Solutions

Change Record

Revision	Date	Description	Reviewer
1.0	6 th May 2021	Initial Draft	Chloe Richards, Adrián Delgado Ollero
1.1	11 th May 2021	Second draft	Fiona Regan
1.2	23 rd May 2021	Third draft	Célia Mercader
1.3	25 th May 2021	Fourth draft	Asa Eitan
1.4	28 th May 2021	Fifth draft	Dulce Muñoz
1.5	28 th May 2021	Sixth draft	Yan Delauré
2.0	1 st June 2021	Seventh draft	Dulce Muñoz
2.1	2 nd June 2021	Eighth draft	Asa Eitan
2.3	3 rd June 2021	Final draft	Yan Delauré
2.4	25 th Nov 2021	Added 3 additional authors which were not included in the final draft	Pablo Benguria



1.0 Executive Summary

The NEMMO Research and Innovation Action project is funded by the European Commission under its Horizon 2020 framework programme. The project was approved under call LC-SC3-RES-11-2018: Building a Low-Carbon, Climate Resilient Future: Secure, Clean and Efficient Energy. This Deliverable 3.4 describes key findings from research carried out to develop novel solutions for enhanced material performance of composite turbine blades for application in tidal stream power conversion. This work is now complete, and the report is intended to summarize key results. An outline of methodologies developed and implemented are presented first. Key test results are then summarized. Three important aspects of composite blade design and construction are addressed in turn in the report following the first three tasks of the Work Package.

Task 3.1 is about reinforcement of conventional composite materials used for making blades by particles such as carbon nanotubes or impact modifiers. These fillers will increase the fatigue life as well as mechanical properties.

Task 3.2 focusses on anti-fouling strategies inspired by skin topography of a marine flat fish. Five candidate textures were selected for their potential to disrupt biofilm formation and reduce the attachment strength of micro-organisms at the early stage of settlement. The surfaces were tested in the lab under controlled conditions. Static immersion tests were aimed at determining the impact of surface micro-texturing on settlement. Single species tests have been performed to identify the percentage of surface coverage and the characteristics of colony formation after immersion. Results have confirmed the propensity of organisms to settle where multiple attachment points are accessible. A significant reduction in settlement over exposed crest planes has been observed. While single isolated organisms and clusters have been found in the groves between raised topographies or in the recessed cavities, the gap size in the topography has been shown to exclude larger organisms and a lower rate of settlement is clearly achieved both in the groves and overall.

Two synthetic approaches (based on 2K fluorinated and acrylated polyurethanes and 1K aqueous cationic PUDs) were followed by FUNDITEC for the development of permanent non-leaching anti-fouling coatings in Task 3.3. Two types of nanoparticles (functionalised biocide nanoparticles, synthesised by TECNALIA and carbon nano-complexes prepared by SPNANO) were incorporated into the developed PUR matrixes and formulated for their application on composite coupons developed by CANOE. An in-depth study was carried out to obtain the best conditions for the preparation of stable dispersions of nano-complexes, provided by SPNANO with different carbons (graphene, CB, CNTs) and the SP1 protein and the two types of components in FUNDITEC's formulations. Mechanical properties (adhesion and hardness) seem not to be improved neither diminished upon the inclusion of any of the two types of nanoparticles. The samples coated with functionalised silica nanoparticles were tested following the ASTM D6990-05 standard which confirmed the effectiveness of the antifouling solution. The highest concentration of nanoparticles provided the best performing solution, but this is achieved to the detriment of the adherence to substrate. Regarding erosion resistance, it seems that the developed coatings show better resistance to erosion than commercial ones. Coating 15 and PUD5 performed the best (about 0,02% mass loss). Incorporation of carbon and silica nanoparticles into the PUR matrixes has no significant effect on the resistance to cavitation erosion. Coating15 and PUD5 have been selected as the best topcoat solutions for tidal turbine composite blades waiting for the results of antifouling tests performed by DCU and TECNALIA.



Table of Contents

1.0	Executive Summary	3
2.0	Introduction	7
2.1	Objectives and outline	7
3.0	Nano-enhanced composite materials	9
3.1.1	Carbon Nanotubes (CNT).....	9
3.1.2	The SP1 protein technology.....	10
3.1.3	Impact modifier.....	14
3.1.4	Fabrication of the nano-enhanced composite plates.....	14
3.2.1	Mechanical characterization	15
3.3	Conclusions	19
4.0	Biomimetic anti-fouling surfaces	21
4.2	Surface topography.....	22
4.3	Inspiration from nature.....	22
4.4	Production of marine-inspired surfaces.....	23
4.5	Laboratory and field testing of new bioinspired materials	25
4.6	Image Processing.....	26
4.7	Observations.....	27
4.8	Conclusions	28
5.0	Permanent cavitation resistance, non-leaching anti-fouling coatings.....	30
5.1	Development of biocide functionalised silica nanoparticles. Task 3.3.1. TECNALIA	30
5.1.1	Synthesis and functionalization of silica nanoparticles.....	30
5.1.1.1	Biocide Assay	32
5.1.2	Incorporation of permanent biocide particles into PUR matrix	33
5.1.3	Test Results	34
5.1.3.1	Roughness and contact angle	34
5.1.3.2	Adhesion to the substrate and hardness by pencil	35
5.1.3.3	Biofouling resistant by exposure on sea immersion conditions (Pasaia's Port).....	35
5.1.4	Conclusions	39
5.2	Development of highly crosslinked PUD containing cationic co-polymers and particles for cavitation and antifouling resistance. Task 3.3.2. FUNDITEC.	40
5.2.1	Introduction	40
5.2.2	2K fluorinated polyurethanes.....	40



5.2.2.1 Synthesis	40
5.2.2.2 Formulation of coatings and application on glass substrates.....	41
5.2.3 1K cationic polyurethane dispersions	42
5.2.3.1 Synthesis	42
5.2.3.2 Formulation of coatings and application on glass substrates.....	43
5.2.4 Incorporation of nanoparticles into the polyurethane matrix	43
5.2.4.1 Incorporation of carbon nano-complexes.....	43
5.2.4.2 Incorporation of functionalised silica nanoparticles	46
5.2.5 Application of coatings on composite substrate	47
5.2.6 Characterisation of coatings.....	48
5.2.6.1 Mechanical properties	48
5.2.6.2 Cavitation erosion tests.....	49
5.2.7 Conclusions	51
References.....	53



INTRODUCTION



2.0 Introduction

2.1 Objectives and outline

This deliverable describes the novel composite material solutions developed by the NEMMO consortium to enhance the resistance of marine tidal turbine blade. Key test results are presented along with an outline description of methodologies adopted. The Work Package targets three parallel approaches adopted to enhance blade material performance. Each refers to a separate Task and is addressed in turn in the report.

Task 3.1 targeted new nano-enhanced composite material solutions to improve fatigue and impact resistance. Task 3.2 focused on the design and testing of biomimetic texture solutions to control biofouling. Task 3.3 was concerned with the development of non-leaching coatings incorporating biocide nano-particles to enhance both cavitation and biofouling resistance.

The report follows the same structure as outlined below:

- Section 1: Introduction. Main purpose and structure of the report.
- Section 2: Nano-enhanced composite materials.
- Section 3: Biomimetic surfaces.
- Section 4: Nano-enhanced coatings.

The document is intended for all stakeholders and for public dissemination.



**TASK 3.1 NANO-ENHANCED COMPOSITE MATERIALS FOR
ENHANCED FATIGUE AND IMPACT RESISTANCE**



3.0 Nano-enhanced composite materials

3.1 Fabrication of composite materials

The objective of this research into novel composite material formulations is to enhance mechanical properties such as fatigue and impact resistance of the tidal blades. The strategy is to add nanoparticles inside the resin or/and at the surface of the glass fabrics.

Two kinds of nanoparticles were selected in order to develop innovative formulations to increase wear resistance, fracture toughness and cohesive behaviour.

3.1.1 Carbon Nanotubes (CNT)

Carbon nanotubes are well known for improving mechanical properties (fracture toughness properties and fatigue resistance) at low concentration (<1%). Several studies have shown their positive effects in epoxy-based composites for off-shore energy applications yielding to a longer operating life and a better reliability [1]. Some mechanical measurements were done on epoxy/CNT composites to compare with a neat epoxy composite. The conclusion is that compared to the reference, composites with CNT have a longer fatigue life under identical conditions. The enhancement in fatigue life may occur by pull out of the CNT and crack bridging at the crack interface [2]

In the NEMMO project, CNT are used via a ready to use masterbatches. A masterbatch is a solid additive with well dispersed CNT at high concentration in a thermoset (in this case) matrix to be dispersed in a liquid thermoset (NEMMO resin). The masterbatch is diluted with the NEMMO resin in order to achieve the targeted concentration. These masterbatches have been designed so as to be mixed in the standard processing conditions of materials, in which they will be introduced with commonly used industrial tools.

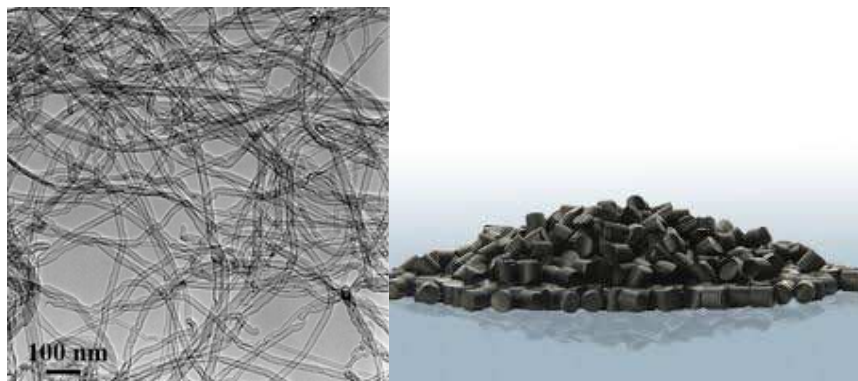


Figure 1. [Left] : SEM picture of carbon nanotubes; [Right] : picture of a masterbatch containing 25% of CNT.

For the NEMMO project, masterbatches are ordered from ARKEMA (tradename of the CNT: graphistrength®) and 2 different masterbatches are evaluated, as there is no masterbatch specially designed for vinyl ester resin:

- CS1-25 : for epoxy-based materials
- CPU-30 : for polyurethane based materials



The carbon nanotubes are introduced inside the resin before the composite processing using a three roll mill, which is a high shear mixer that ensure the good dispersion of the CNT inside the resin without aggregate.



Figure 2. Dilution of CNT-masterbatch in NEMMO resin using 3 rolls mill.

SP NANO has also developed solutions containing carbon nanotubes: they consist of nano-complexes between CNT and SP1 protein, a 12 reactive sites bio-engineered protein that enhances dispersion of CNT within different matrixes.

The nano-complexes will be used as a direct coating at the surface of the glass fibres and will be applied by impregnation of the glass fabrics inside the nano-complexes solution. This should lead to reinforced interlaminar protecting against un-folding and delamination. The nano-complexes can also be used by direct dispersion into the resins leading to strong interactions with the composite resin.

Based on previous implantation with epoxy and phenolic resin with carbon fibers, 50% stronger composites parts, 20°C increase in Tg, 180% stronger adhesion and 100% of improvement in fracture toughness were observed. Also, the adhesive failure turned to cohesive failure.

3.1.2 The SP1 protein technology

- SP1 originally isolated from the Aspen tree is a boiling stable protein. It is also resistant to detergents, organic solvents and proteases, rendering it suitable for many industries with a low cost of production by an industrial fermentation.
- SP Nano has genetically engineered the exceptionally stable protein, SP1, to become a specific tailored solution for carbon nanoparticles (CNP) (e.g., Multi/Single-Walled Carbon Nanotubes (CNT), graphene and carbon black (CB)).
- The engineered SP1 presents 12 times on its surface a peptide specific for graphitic surfaces and therefore binds very tightly to CNPs resulting in extremely stable dispersions of high concentrations.
 - The tight binding is derived by simultaneous binding by 6 peptides, while each peptide contain several binding sites (Fig. 3)
 - Once bound to the CNP, the protein will not release its binding



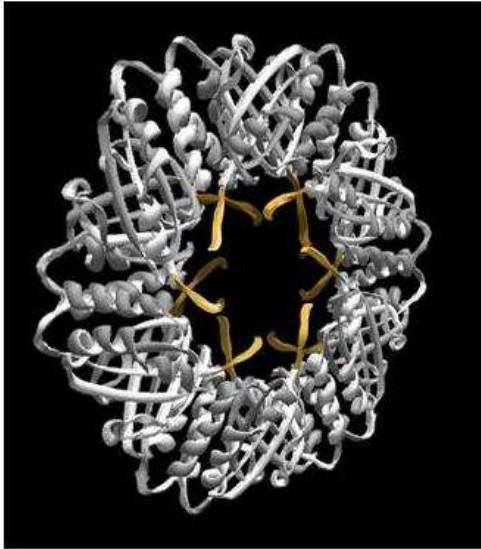


Figure 3. The crystal structure of SP1 reveals a ring like structure. The yellow ribbons represent the graphitic binding peptide which is presented 6 times on each side of the ring. The peptide enables the protein to dock with high avidity on carbon nanoparticles. The rest of the protein's surface can be involved in many other potential interactions with polymers and small molecules of choice to adapt the SP1/CNP complex to different chemical environments.

Without the need for chemical modifications (that disrupts the molecular structure of CNPs and therefore compromising their properties) or detergents (that are needed in high amounts and interfere with downstream applications) the SP1 technology provides the best dispersions of CNT and graphene comparing to the state-of-the-art, thereby, unleashing the huge potential of these nanoparticles in applications that require excellent mechanical properties, wear resistance and thermal and electrical conductance, e.g., batteries, supercapacitors, conductive inks coatings, adhesives, composites, paints, smart textiles etc. with properties that include:

- Higher dispersion level
- Higher stability
- Reduced viscosity
- Increased solid content
- Low SP1 to CNP ratio
- Stronger affinity
- Pristine CNP

SP1 enables two approaches for composites nanoreinforcement:

- Dispersion in resin
- Fibre coating

The SP1/CNP complex binds to fibres of textiles, e.g., glass fibre as used in NEMMO. In composites, fibre coating and/or matrix reinforcement with SP1/CNP improves the inter-laminar mechanical properties:

- Enhancing fibres to resin bonding, leading to efficient load transfer
- Arresting crack propagation, leading to an increased fracture toughness
- Overcoming delamination issues caused by adhesive failure, enabling complex fibers-matrix combinations



SP1 binds covalently to matrices such as epoxy, phenolic etc.

- SP1 comprises a variety of functional groups that facilitate a diverse chemistry with different resins
- In epoxy or phenolic resins, the multitude of amine groups of SP1 create covalent bonds with the matrix, which together with the tight binding of the CNT itself, guaranteeing that the CNT will be torn and not pulled out, thereby serving as a true nano-reinforcement (Fig.4)

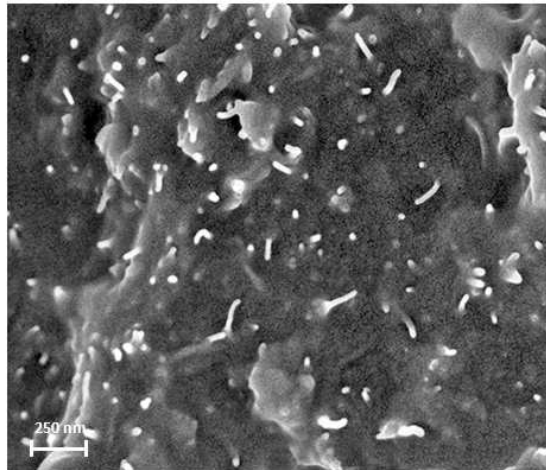


Figure 4. HR-SEM of fracture surface of epoxy reinforced with SP1/MWCNT after T-Peel. It is evident that: 1. the CNTs are homogeneously dispersed; 2. All the CNTs are torn at or close to the fracture surface, indicating that they were participating in the effort to prevent the crack propagation; 3. While epoxy fracture surfaces are usually smooth, the rough surface in the image indicates that the crack propagation in the treated material was interrupted by the CNTs.

To improve properties of the NEMMO blade, SP Nano has used its graphitic surfaces specific, genetically engineered protein, SP1, first, as a dispersant, to develop and optimize protocols for dispersion processes of different representative types of carbon nanoparticles (CNPs), i.e., SWCNT, MWCNT, long MWCNT, CB, graphene.

In order to lower the chances for adhesive failure of the composite, an approach of nano-reinforcement of the interface between the fibers and the matrix was taken.

SP1 is responsible for dispersing the CNPs and, then, for binding them to the GF. The parameters critical for coating the different glass fabrics used in Nemmo were explored.

Nano-complex of SP1/MWCNT were applied as a homogenous nanometric coating to the fabrics, including different loads of MWCNT and MWCNT complexed with latex particles.





Figure 5. Visual inspection of the coating: homogeneous.



Figure 6. Light microscopy doesn't show any aggregate.

The following graph summarizes lightness measurements of some of the coated fabrics (In colorimetry and color theory, lightness, also known as value or tone, is a representation of a color's brightness). The higher the CNP load on the fabric, the darker its appearance (lower lightness).

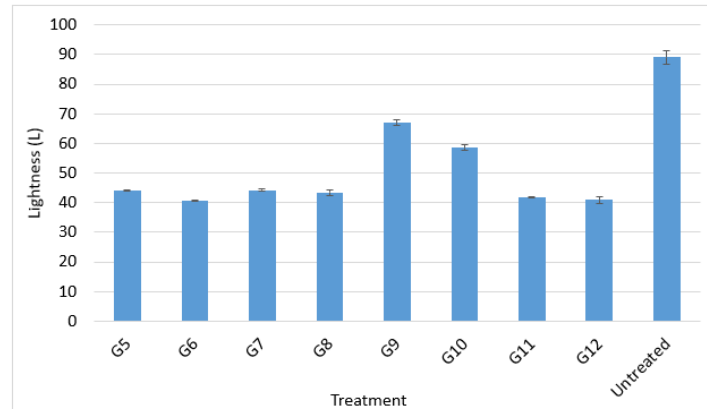


Figure 7. lightness measurements of fabrics coated using different conditions (particles, concentration, ...)

3.1.3 Impact modifier

XT100 is a core shell additive consisting of methylmethacrylate-butadiene-styrene (MBS). It is particularly recommended to increase toughness of polyester-based polymer formulation for composite.

The impact modifiers can be directly mixed inside the resin without specific tools.

Studies have shown the positive effect of impact modifier block copolymers onto the impact properties of epoxy-based composites. The impact modifier has improved the toughening properties as well as impact absorbing properties of epoxy resin without lowering the glass temperature.

3.1.4 Fabrication of the nano-enhanced composite plates

The composite process used to manufacture the samples is a liquid resin infusion process:

First, the resin is mixed with the appropriate ratio of nanoparticles concentrates and mix with a static mixer to reach the targeted concentration. The glass fabrics are cut to the required dimensions. The technical fabrics (peel ply, vacuum bag, external draining and resin tracks) are added. The system is then put under vacuum and the resin is added (after addition of the accelerator and the catalyst). The composite is then cured as recommended on the data sheet of the resin.





Figure 8. Picture of infusion process.

For each developed formulation, 4 plates are manufactured for mechanical characterizations.

3.2 Characterization and results

Concerning the addition of charge, there is no filtration of the charge by the fabrics during the infusion process. This means, that the composite plates are homogeneous.

Also, with the highest load ratio at particles, it appears that the increase of viscosity of the resin is too high for the infusion process. The concentration of particles had to be reduced.

3.2.1 Mechanical characterization

Materials have been tested following the test matrix shown in Table 1.

Table 1. Mechanical characterization test matrix and standard associated

Test	Standard
Traction 0°	ISO 527-5 Type A
Traction 90°	ISO 527-5 Type B
ILSS	ISO14130
Traction +/-45°	ISO14129
Charpy	ISO 179

Mechanical tests at 0° and +/-45° are carried out on an allround ZWICK/ROELL Z250 machine equipped with a 250kN force sensor and with both a mechanical extensometer (gauge length 25mm) and digital image correlation (Cf. Figure 9). For traction at 90° an allround ZWICK&ROELL Z010 equipped with a 10kN force sensor and a mechanical extensometer (gauge length 20mm) is used.



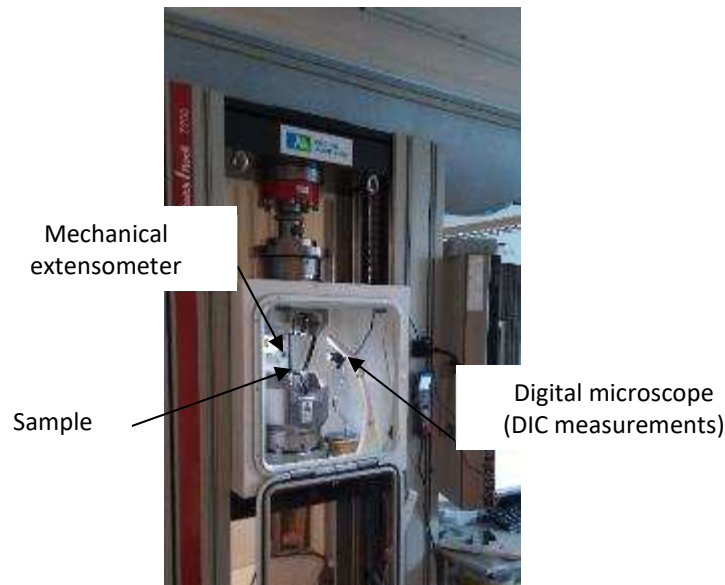


Figure 9. Experimental setup for traction test.

For the 0° and $\pm 45^\circ$ traction tests, failure is too energetic to let the extensometer on the sample until failure, so that a 2 steps process is adopted:

- First step: the material is loaded until 0.3% strain is achieved and then unloaded. This first step, during which the extensometer measured the strain, is used to measure elastic modulus – E (between 0.05% and 0.25% deformation).
- Second step: the material is loaded until it breaks. This second step is used to assess the maximum stress – σ_{\max} . During this step, strain is calculated from the traverse displacement (note that this method to assess strain is less precise than extensometer measurement).

Tensile properties for traction in the direction of the fibres are shown Figure 10. The modulus and the maximum stress are not really influenced by the nature of the filler in the resin. This can be explained by the fact that the mechanical behaviour is mostly influenced by fibre behaviour.



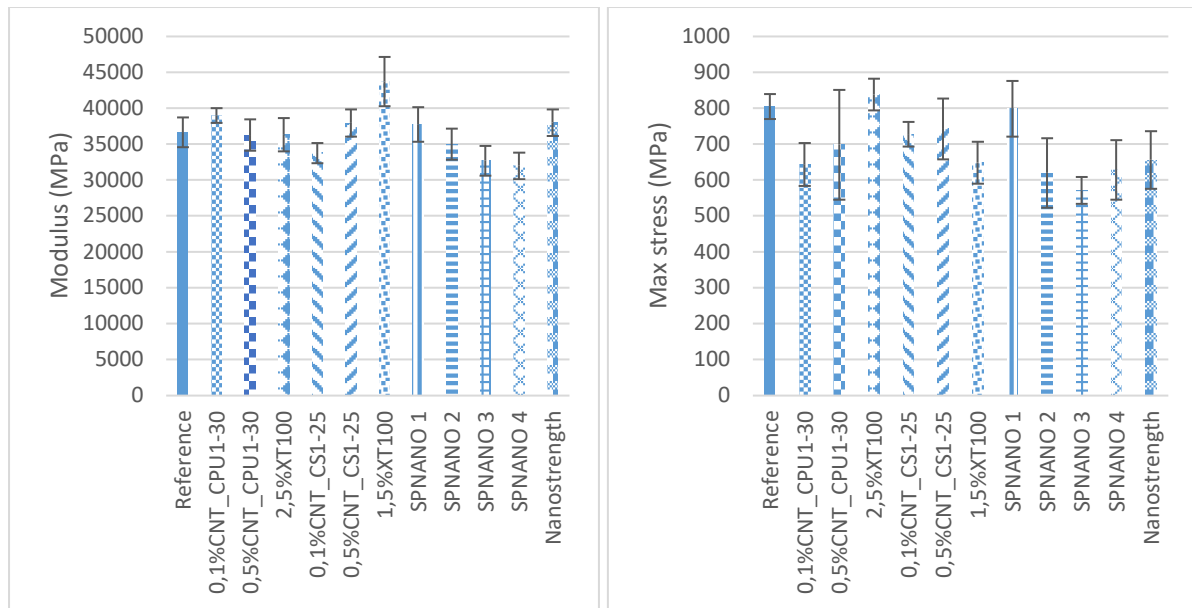


Figure 10. Modulus and max stress for 0° tensile tests on the different formulated materials as molded

For 90° traction tests, as failure is less energetic, an extensometer is used until the failure of material and the test is carried out with one step.

Tensile properties for traction perpendicular to fibre direction are shown Figure 11. There is about 10% modulus increase with fillers, whatever their nature. This increase is not seen on SP NANO’s glass fibre preparations composites where same or smaller modulus is measured. The maximum stress obtained does not change function of the filler.

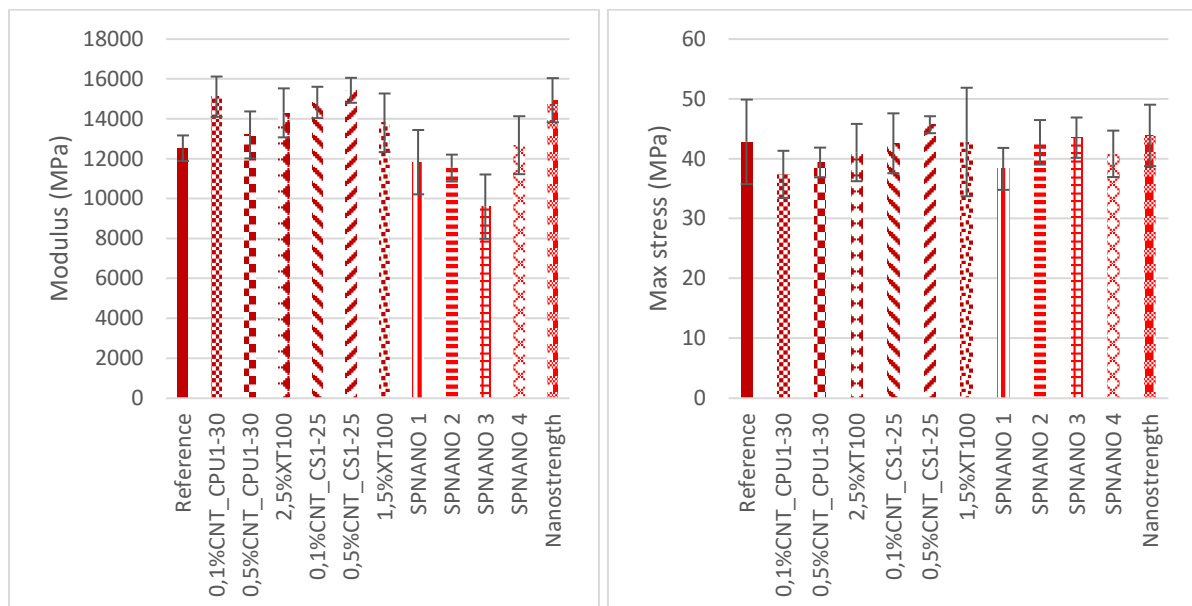


Figure 11. Modulus and max stress for 90° tensile tests on the different formulated materials as molded



Interlaminar Shear Strength (ILSS) tests are carried out on an allround ZWICK/ROELL Z010 machine. The shear failure mode is controlled with a digital camera (Cf. Figure 12.).

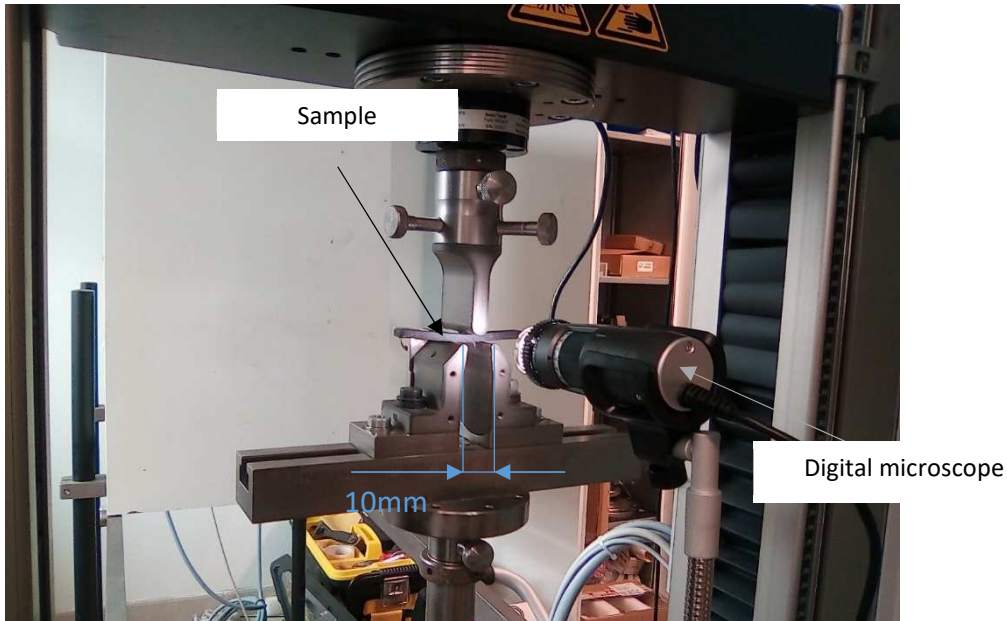


Figure 12. Experimental setup for ILSS tests

ILSS results are shown in Figure 13. They show significant improvement for XT100 and CNT_CS1-25 (up to 25% improvement for both 0.5%CNT_CS1-25 and 2.5%XT100). For both formulations there is a significant effect of filler concentration (the more concentrate, the stronger). However, by mixing CNT and XP100, no synergetic effect can be seen.

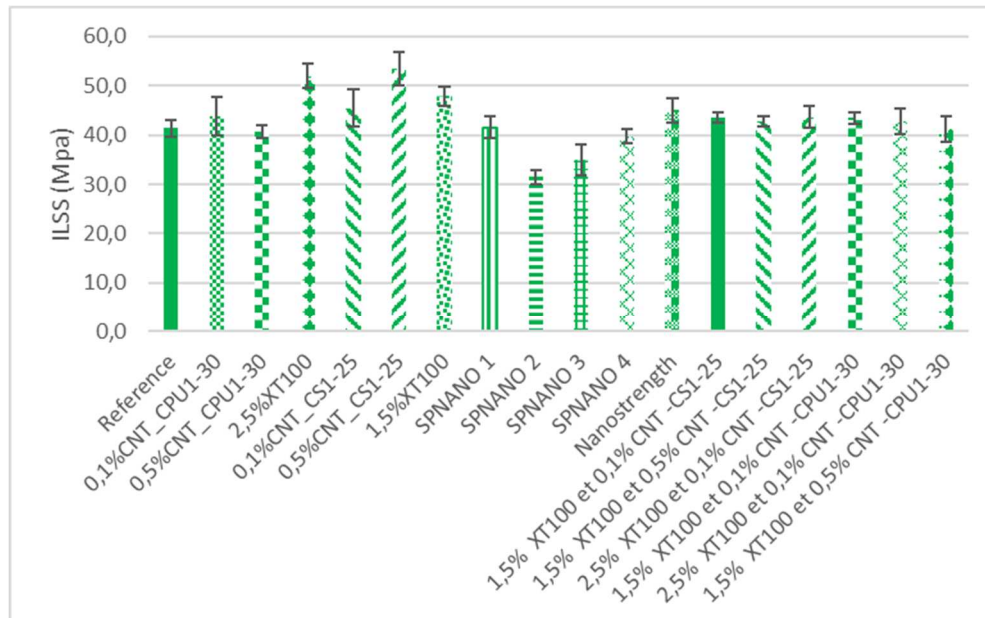


Figure 13. ILSS of the different formulated materials as molded



3.3 Conclusions

Several formulations including CNT and impact modifiers added to the reference resin have been tested. Composite plates of glass fibre reinforced vinylester resin have been successfully manufactured for each formulation. Mechanical characterisation of each composite including in plane characterisation (longitudinal, transverse, +/-45° tensile traction), ILSS and Charpy impact testing have been done. There is a strong dependency of the formulated resin for ILSS and +/-45° tensile tests (in-plane shear). Other mechanical properties seem to be similar whatever the formulation. The best results are achieved with the highest concentration of both 0.5% CNT_CS1-25 and 2.5wt% XT100 formulations (+15% in tensile max stress for +/-45° and +25% in ILSS).



TASK 3.2 BIOMIMETIC SURFACES TO CONTROL ANTI-FOULING



4.0 Biomimetic anti-fouling surfaces

4.1 The challenge of biofouling

Biofouling, the development of nuisance or unwanted biofilms on surfaces is a major problem due to accumulation of biomass causing reduced efficiency, contamination, corrosion, and failure of engineered components. Fouling in the marine environment has been an issue that has reduced the lifespan of structures, increased the fuel consumption of vessels, increased maintenance frequency and spread invasive species for as long as mankind has been placing objects in the water [1].

Biofilm formation is most readily recognised in marine and freshwaters environments where a cursory glance at a surface such as a ship's hull immersed for even a short period (weeks) reveals a multitude of organisms attached to and populating surfaces.

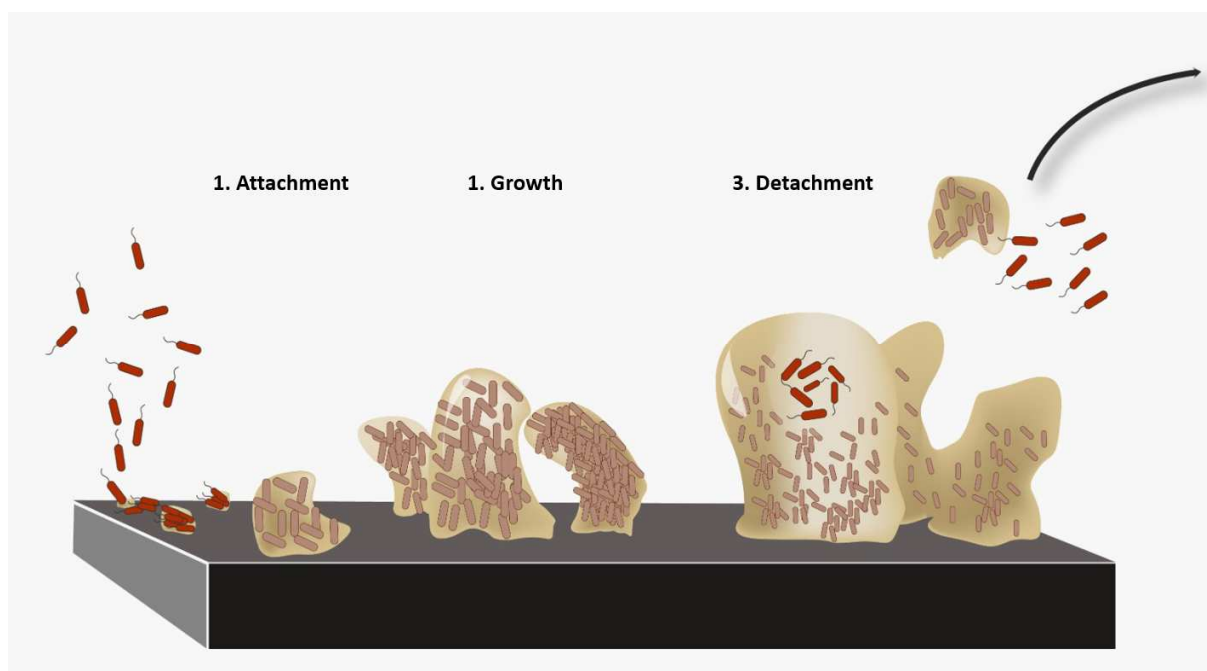


Figure 14. Biofouling begins with the conditioning of the surface with organic substances like proteins and carbohydrates before microscopic organisms settle and develop into a layer of microorganism known as a biofilm, this is generally followed by the settlement and proliferation of macroscopic organisms. This trend is general and macrofouling organisms can settle and grow on surfaces free from biofilms, but a number of studies have shown macroscopic organisms have preferences for biofilm conditioned surfaces and even have preferences for biofilms composed of specific organisms. Due to their larger size, mass and adhesion strengths, macrofoulers have a greater impact on the function of surfaces but microfouling is still detrimental to submerged structures. (Adapted from the Center for Biofilm Engineering at MSU-Bozeman [2])

Fouling involves the accumulation of unwanted material on a surface. This material can comprise of either organic, or inorganic compounds, or a wide range of organisms ranging in size from individual bacteria to barnacles, which in turn can produce complex multi-dimensional and multi-species communities (Figure 1) [3]. Marine biofouling starts immediately after the immersion of a surface in water and begins with the adsorption of organic molecules (i.e., nucleic acids, carbohydrates, and



proteins. This coating helps the adsorption and growth of fouling organisms. Biofouling organisms are categorised into three groups [4], [5].

- microfoulers (i.e., microorganisms) e.g., bacteria, diatoms, and microalgal biofilms
- soft macrofoulers (i.e., macroalgae), e.g., sponges, bryozoans, and multicellular algae
- hard macrofoulers, (i.e., barnacles and mussels)

The cell response towards a surface is thought to be dependent upon the physio-chemical characteristics of that particular surface. Microbial responses to change in the chemical nature of surfaces and material properties are commonly well known [6], [7], while microbial response to surface topography is relatively less well understood. Detailed analysis of the effect of these topography properties is thus a necessity in developing a targeted design methodology for antifouling applications. Research in this direction has gained footing in recent years, leading to better understanding of interactions between topography, adhesion and the settlement of microbial organisms. However, the wide range of organisms involved, varying and incompletely characterised surface topography, and the multitude of settlement configurations possible for colonising cells, often requires complicated quantitative analysis of these interactions. Furthermore, microbial adhesion in the natural environment consists of multiple species simultaneously competing for space on surfaces. The issue thus arises as to influences of inter-species and inter-cellular interactions on microbial settlement on topographic surfaces and distribution of cells on the surface. Aside from the influences of surface topography on individual cells, the development of microbial communities at interfaces has in itself been a relevant subject of research for several decades.

4.2 Surface topography

In recent years, the study of surface topographical features has become increasingly popular, with several investigations reporting sophisticated natural topographies found on many organisms that are known to have antifouling properties. The replication of artificial surfaces inspired by nature has produced many promising results [7]–[11]. Studies have shown a mixture of attachment, depending on the size and shape of the organism and the specific microtexture used as a fouling-resistant mechanism. However, the explanation behind this attachment is still not well known. Numerous theoretical models have been proposed through the years to in order to understand this attachment behaviour. One of these models is attachment point theory (APT) [12], [13]. In this model, the fouling organism experiences increased attachment where there are multiple attachment points and reduced attachment when the number of attachment points are decreased. This can often be related to microtexture in the sense that highly intricate topographies (i.e., whereby the microtexture is smaller than that of the organism) will not be favourable for attachment. On the other hand, where the microtexture is larger than the organism, settlement does occur [14]. The work of Lorenzetti et al. confirms previously mentioned examples about the correlation between bacterial adhesion and a substrate [15], [16].

4.3 Inspiration from nature

Surfaces from marine organisms capable of lowering or inhibiting biofilm formation are of interest in engineering and materials sciences [16]–[19]. Biomimetic surface modification has been considered in antifouling material development and a number of studies have examined the antifouling ability of topographic patterns, textures and roughness scales found on these organisms [18], [20], [21]. The surfaces of many marine animals (i.e., mollusc shells, shark skin, and crustaceans) feature complex



topography. These topographies have a role in antifouling, either by deterring organisms from attaching, or encouraging their easier release [22]. It can also be said that these marine organisms have evolved to present physical, behavioural, and chemical mechanisms that display these antifouling properties [23]. In that respect, the processes used by marine organisms to prevent fouling on external surfaces is worth further investigation.

Scophthalmus rhombus (Brill), is a small flatfish occurring in the marine waters of the Mediterranean as well as in Norway and Iceland. It inhabits sandy and muddy coastal waters from 5 to 80 metres. Its skin changes colour depending on the environment but is generally brownish with light and dark freckles and a creamy underside. *S. rhombus* is oval in shape and its flesh is white [24], [25].

The design of a micro-texture to control fouling was inspired by the growth rings of the brill fish, *Scophthalmus rhombus*, characterised by arrays of individual separated micro-ridges of average length, 74.9 μm , and height, 11.7 μm , with peak-to-peak distance between neighbouring parallel ridges, 16.6 μm and intervals between successive features, 15.8 μm . A typical array viewed by SEM is shown in Figure 15.



Figure 15. A typical array of the growth rings of the brill fish, *Scophthalmus rhombus*, viewed under scanning electron microscopy (11.0 mm, x42, 20 kV).

4.4 Production of marine-inspired surfaces

Over the past number of years, developments in technologies to produce surface topographies at the micro- to nano-scale level have grown enormously and allowed for numerous “cell-surface interaction studies” [26]. Many different surface topographies at both the micro- and nano-scale level (i.e., channels, pillars, riblets, pits) were achieved through the use of different manufacturing methods [26]. In this work, the micro-texture was produced using a 3-D printing process. The steps in the development of the micro-texture can be described in the following way (Figure 16):

- **Characterization** – Six different dimensions of micro-ridges, formed by the interruption of rings by ray-patterns were considered, measured using Image J software. Each dimension



was assigned a letter, with average dimensions calculated from a number of SEM micrographs, from four different samples and from different scales.

- **Design** – The design was constructed using modelling software, SolidWorks 2017. The key feature of the design was to replicate the separated micro-ridge with several slight modifications both in terms of measurements and shape. The cross section of the scale was replaced with a rectangular design for increased mechanical stiffness, replacing the sharp edge of the ridge with a flat surface of width, $10\ \mu\text{m}$, and length, $85\ \mu\text{m}$, to reduce machining requirements.
- **3-D Printing** – The textures were reproduced using the Nanoscribe Photonic Professional GT 3D printing system (Nanoscribe, GmbH), which uses a direct laser writing process whereby polymer structures are formed by deflecting a laser beam into a photosensitive material using alternating X and Y laser scanning directions.

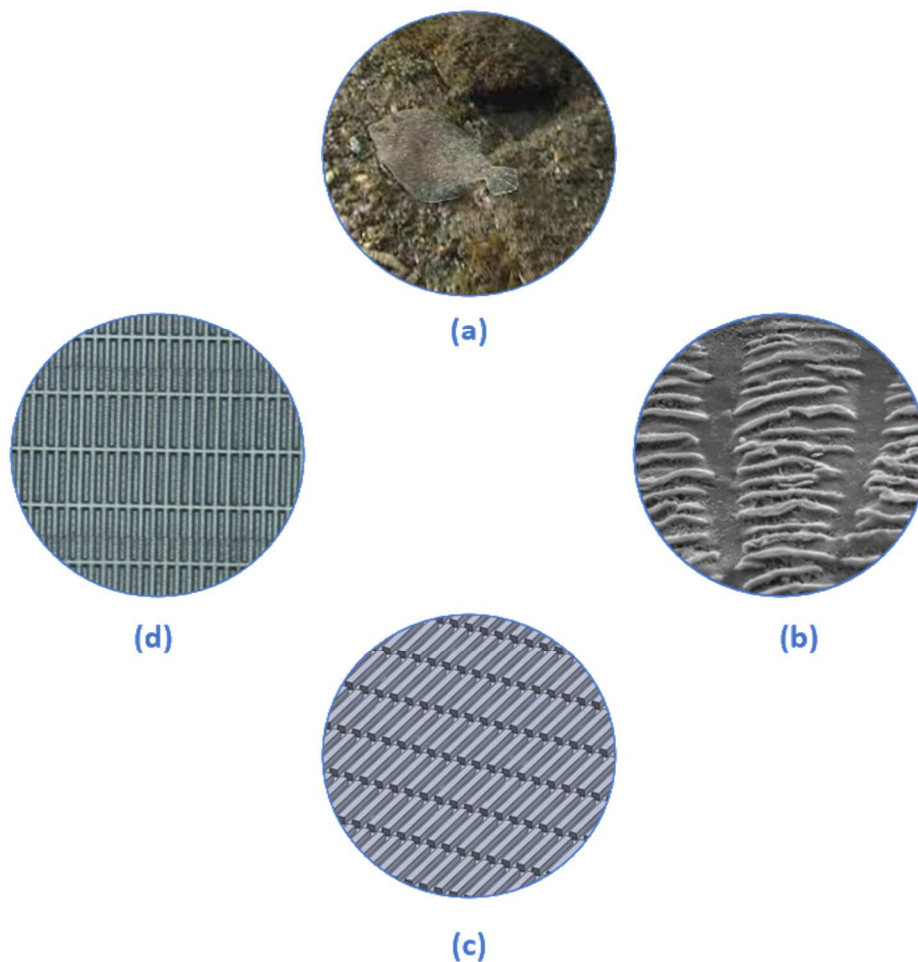


Figure 16. The process of micro-texture development. The design of the micro-texture was inspired by the growth rings of the common brill fish, *Scophthalmus rhombus* (image sourced from shutterstock.com) (a). The micro-topography of the brill fish was characterized using a series of SEM micrographs and Image J software (b), and constructed in SolidWorks 2017 (c). Micro-textures were produced using a nanoscale 3-D printing process called the Nanoscribe Photonic Professional GT 3D printing system (d).



4.5 Laboratory and field testing of new bioinspired materials

The organisms used for laboratory tests of the materials were *Halamphora coffeaeformis* and *Nitzschia ovalis* from the Culture Collection of Algae and Protozoa of the Scottish Marine Institute. They were grown in water with filtered sea salt and supplemented with nutrients for Guillard's F/2 + Si medium. The cultures were first conditioned. The cultures were grown in a 'batch' growth system in 5L Pyrex bottles, in a temperature range of 15 °C to 23 °C and with a 12:12 light: dark cycle, with continuous light of 65 $\mu\text{moles}/\text{m}^2/\text{s}$. The cultures were homogenised with filtered-air supplied by pumps and soft bubblers. Cell concentration was monitored using optical density (O.D. 750nm) using a UV-Visible Spectrophotometer, keeping the cells in the exponential growth phase in the range of 0.3 – 0.5 AAU. Cell numbers were estimated by counting using a light microscope and an improved Neubauer bright-line haemocytometer (0.1 mm depth, Sigma, Ireland). Cells were diluted with 0.45 μm artificial sea salt to achieve a cell density of approximately 3×10^6 cells per mL for use in adhesion assays.



Figure 17. Test organisms: *Halamphora coffeaeformis* (left) and *Nitzschia ovalis* (right) (imaged sourced from the Culture Collection of Algae and Protozoa, SAMS Limited, Scotland, U.K. (image sourced from the Culture Collection of Algae and Protozoa, SAMS, Scotland, U.K.).

Laboratory assessment of bioinspired materials was performed using a 10 mL culture suspension of fouling organism, *Nitzschia ovalis*. The textures were firstly purged with N_2 gas to remove air pockets. Microtextures were immersed in the cell suspension for 3 hr in individual petri dishes. Colonization of textures was observed by removing the microtextures from the cell suspension and dipping twice sequentially in solutions of 50:50, artificial seawater: deionised water and deionised water. Samples were stained by immersion in $10 \mu\text{g mL}^{-1}$ of acridine orange (AO) dye for 3 min at room temperature. Samples were rinsed three times sequentially in deionised water to remove excess stain and allowed to dry. The colonization of organisms on the candidate microtextures was observed using the Keyence VHX2000E 3D digital light microscope with high resolution zoom lens VH-Z500R (500 x to 5000 x). Images were acquired at a magnification of 500 x from each candidate microtexture, control and ITO-coated glass sample (n=3).

Field testing was used to assess the growth of a biofilm on smooth glass microscope slides over a 12-month period. The site chosen for the deployment was that of Poolbeg Yacht & Boat Club, Dublin Bay, Ireland (53.3421°N, 6.1513°W) (Figure 18). Poolbeg Yacht & Boat Club lies in the centre of Dublin, close to Dublin Port, on the southern side of the River Liffey. 90 glass microscope slides were deployed off a pontoon at Poolbeg Yacht & Boat Club. Biofilm was characterised each month for protein and carbohydrate using a series of biochemical assays. Diatom communities were identified using scanning



electron microscopy to determine the most common fouling organisms present in the marine environment.



Figure 18. Left: Satellite imagery of the deployment location at Poolbeg Yacht & Boat Club, Dublin. Right: Images of triangular deployment cage used for housing glass slides (to avoid location effects).

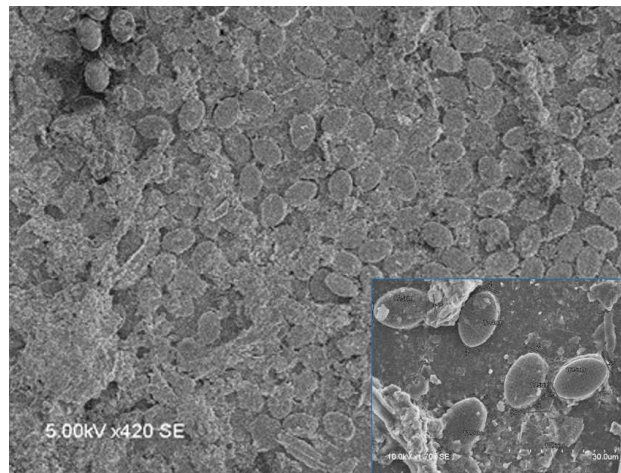


Figure 19. SEM micrograph of the diatom genus, *Cocconeis*, completely colonising the surface of a smooth glass microscope slide.

4.6 Image Processing

Image analysis was performed using Fiji (ImageJ) image processing software. The images used in the analysis were scaled to 2.4501 pixels/ μm . Exposure and saturation levels were adjusted to obtain the highest contrast between image elements and images were cropped at 300 x 300 μm using the scale bar in the image in order to remove noise or imperfections such as unwanted particles and material defects. Image segmentation was performed using the Trainable Weka Segmentation (TWS) plugin which uses machine learning algorithms to classify a red-green-blue or greyscale image into different classes. Firstly, the user trained the software by drawing strokes defined as a training set of pixels (STP) over the region of interest (ROI) for each class. An STP of two classes is the minimum necessary for segmentation. Two classes were used. Class 1 corresponds to the particles to be detected, in this case the benthic diatom, *Nitzschia ovalis*, (appearing red). Class 2 corresponds to the background of the image (i.e., textured, and smooth material) (appearing green). This algorithm was chosen because of its computational efficiency, probabilistic output, ability to handle a wide variety of image input



characteristics and interactive enhancement based on error handling. In addition, this algorithm avoids over-fitting the data by injecting randomness in the training trees and combining the output of multiple random trees into the final classifier; in our case 200 trees were performed in each analysis, with an out of bag error lower than 5% to arrive at the final classifier from which a probability map was obtained. The probability map was cropped and processed using an ImageJ plugin to cluster colour pixel driven by the user input developed by Biomedical Imaging Group (<http://bigwww.epfl.ch/>). This ImageJ plugin allows one to segment a colour image by pixel clustering. Five red patterns were used for Class 1 (corresponding to *Nitzschia ovalis*) and five green patterns were used for Class 2 (corresponding to the background). The percentage area covered by each colour was calculated using the K-means clustering algorithm. The analyses were carried out on an individual sample basis. Subsequently, a mean value and a standard deviation were calculated in triplicate.

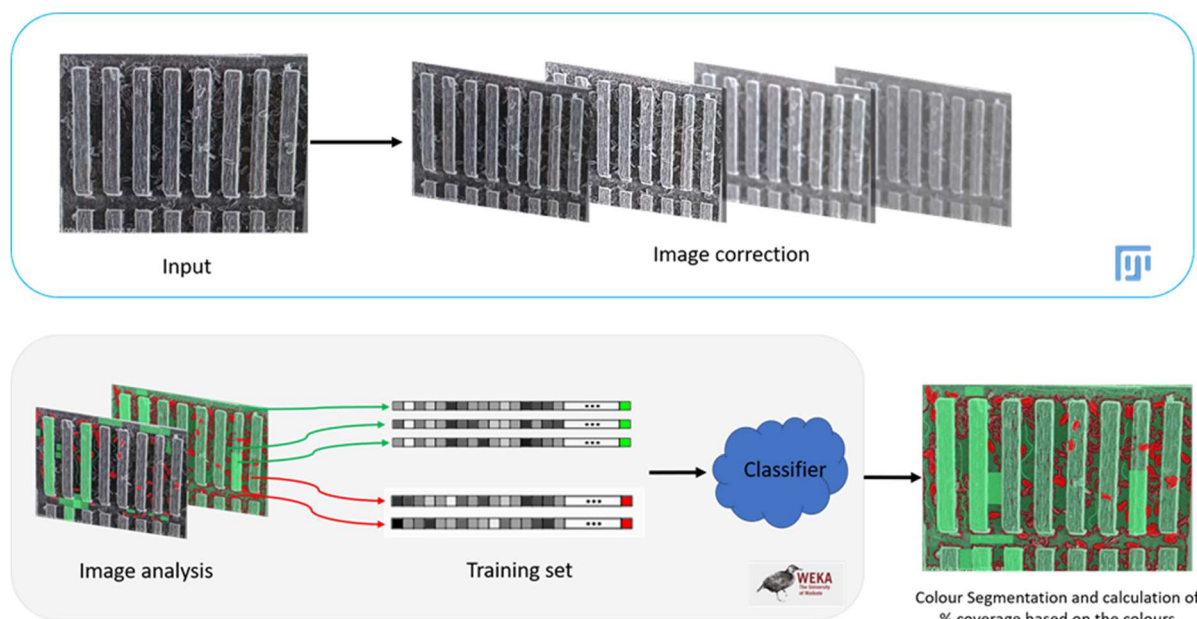


Figure 20. Using Image J image processing software with the trainable WEKA segmentation plugin, the percentage cover of cells on the surface of each of the micro-textures were estimated. 1-way ANOVA was used to test for statistical differences in cell attachment on candidate micro-textures.

4.7 Observations

Figure 40 illustrates the effectiveness of a textured material (right) in comparison with a flat control glass sample (left) to control biofilm development.

On the glass control sample, a large clustering of cell colonies is observed. There is no micro-texture here to break up the colonies of cells and so a high density of cells can be seen populating the surface.

On observation of the textured material, the clustering of cells between uniform gaps of adjacent features appears reduced, with very small numbers of cells adhering on the top of the features, indicating that feature height (L_y) may play a role in deterring cells from the surface. It was noted that some areas of the textured material were completely free from biofouling, while in other areas, smaller colonies are evident. This could be deliberate – by creating a colony, the cells are protected as the force required to dislodge the cells from the surface is greatly increased.



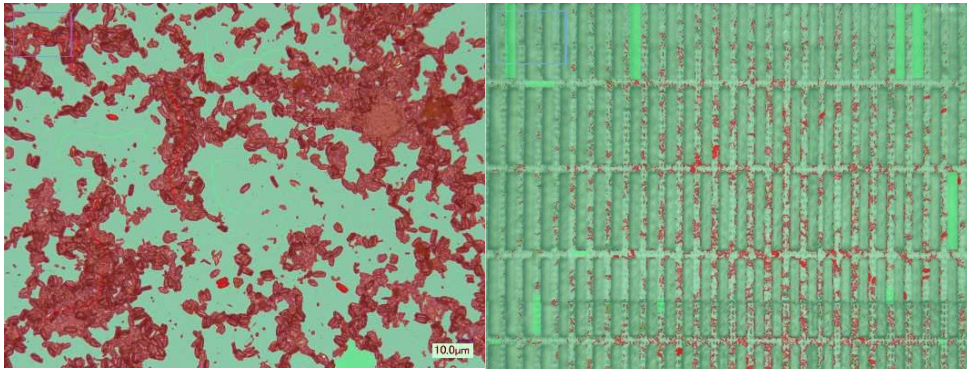


Figure 21. Image processing (arising from ImageJ analysis) illustrating the effectiveness of a textured material (right) compared with a flat control surface of glass (left).

4.8 Conclusions

An application of the micro-texture discussed here is for the control of antifouling on advanced tidal turbine blades. Ocean energy exists in a number of forms including ‘tidal, wave, current, thermal gradient and salinity’. Most research focuses on two forms of ocean energy; tidal and wave energy. In comparison to wind and solar energy, which are affected by weather fluctuations, tidal and wave energy looks to be the most reliable form of renewable energy, providing a constant generation of power [27]. The successful incorporation of antifouling technology onto tidal turbine blades could unlock significant potential for the use of ocean energy, reducing cleaning costs and allowing the extraction of energy from the blade system. Surface texturing has been shown here to be effective under static immersion. Field tests under dynamic are planned as part of a follow on Work Package to assess the impact of hydrodynamic stresses under real sea conditions.



TASK 3.3 PERMANENT CAVITATION RESISTANCE, NON-LEACHING ANTI-FOULING COATINGS



5.0 Permanent cavitation resistance, non-leaching anti-fouling coatings

5.1 Development of biocide functionalised silica nanoparticles. Task 3.3.1. TECNALIA

This task is focused on the development of functionalized silica nanoparticles with biocide activity and the study of their behaviour when they are incorporated in a polyurethane matrix.

5.1.1 Synthesis and functionalization of silica nanoparticles

In this task, a two-step method has been employed for the functionalization of silica particles with biocide moieties. In the first stage, a colloidal dispersion of silica nanoparticles was prepared by addition of TEOS to a solution of absolute ethanol and concentrated ammonium hydroxide (different concentrations were studied). Figure 22 shows two colloidal dispersions which were prepared by adjusting the ammonium hydroxide concentration. This parameter controls the size of the obtained nanoparticles. In these cases, Zeta Potential and particle size obtained by dynamic light scattering (DLS) measurements allowed to conclude that stable dispersions were obtained by this route, with controlled particle size of ~ 30 nm and ~ 75 nm, depending on ammonium hydroxide concentration (**hereinafter SiO₂-30 and SiO₂-75 samples respectively**).

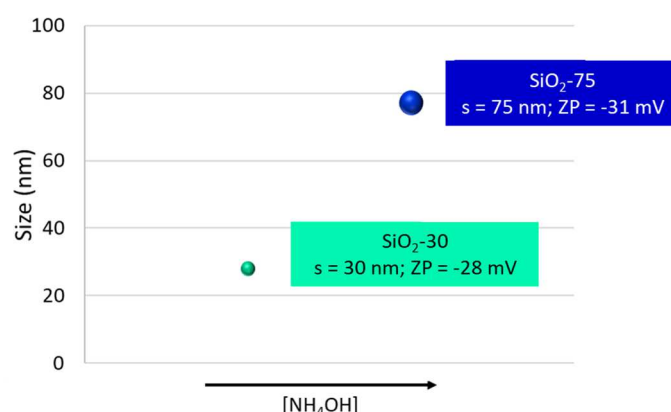


Figure 22. Particle size of intact nanosilica with different concentration of ammonium hydroxide.

After synthesizing intact/pristine nanosilica of two controlled particle size, different quantities of biocide moiety were added to the colloidal suspension. In the case of SiO₂-75, DLS measurements indicated that a colloidal dispersion was obtained without agglomerates and particle size of ~ 85 nm (BF-85 sample). On the other hand, the smaller nanosilica, SiO₂-30, was also functionalised and two particle sizes were detected: one in the nanometric and the other one in the micrometric range/length scale, the former being the most abundant (BF-55 sample). Table 2 shows size and Zeta Potential of selected nanosilica samples.

These four intact/pristine and biocide functionalised nanoparticles were studied by TEM. In the first case (Figure 23), it was observed that the dried size of both intact SiO₂-30 and functionalised BF-55 was in the range of 17-26 nm. Despite the surface modification, the approximate size observed in the TEM images, was found to be similar before and after biocide functionalization. However, the particle size measured by DLS for BF-55 sample showed peaks of ~ 55 nm, which could indicate the formation of small aggregates in the colloidal dispersion. This sample has been discarded for next task (*Incorporation of permanent biocide particles into PUR matrix*).



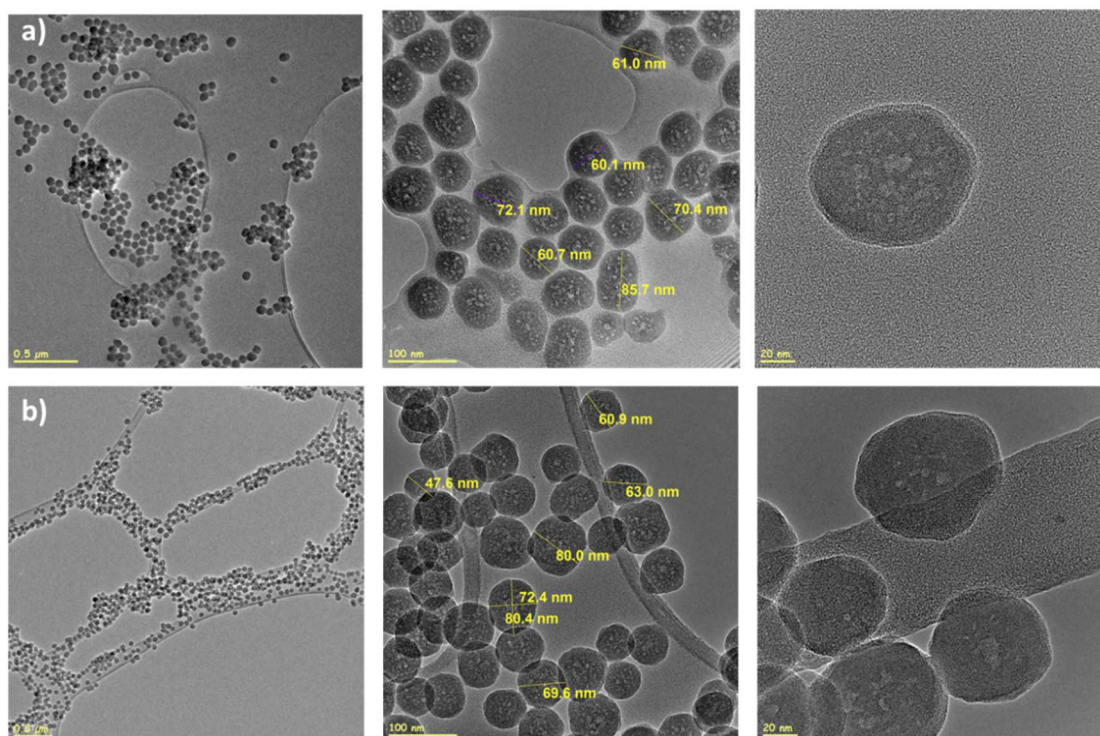


Figure 24. TEM images show the size of intact nanosilica, SiO₂-75 (a) and biocide functionalised silica particles, BF-85 (b).

5.1.1.1 Biocide Assay

The antibacterial activity of the optimized non functionalised/pristine and functionalised silica nanoparticles (SiO₂-75 and BF-85, respectively) was assessed. The biocidal activity of the nanoparticles against *Staphylococcus aureus* was analysed by means of the so-called “Flask Shake Test”. It consisted on immersing the samples in a solution of nutrient broth (1:500) with a known concentration of bacteria (around 10⁵ cfu/ml sample). The bacterial concentration (cfu: the number of colonies forming units) was verified by the pour plate culture method. This method consisted on assessment of the **biocide activity of aliquots of the SiO₂-75 and BF-85 nanoparticles dispersed in water** and placed in sterile petri dishes with Molten nutrient agar and swirled gently. The petri dishes were incubated at 37°C for 24 h and, after the incubation, the colonies present on the plates were counted. The number of viable bacteria in each suspension was determined as cfu/ml.

Viability control *S. aureus* in nutrient broth at the same concentration was incubated without the presence of nanoparticles. After 24 h of incubation at 37°C and shaken, the number of viable bacteria present was measured in each suspension and the antibacterial activity was calculated. The antibacterial activity was determined as the difference between the number of the viable bacteria counts (in logarithmic scale) found after 24 h on the control sample and the viable bacteria counts found in the suspensions that were in contact with the non-functionalised/pristine or functionalised nanoparticles during 24 h (Table 3).



The graph of Figure 25 shows that both SiO₂-75 and BF-85 nanoparticles presented antibacterial activity, against *S. aureus*. However, **functionalized nanoparticles BF-85 showed higher antibacterial activity than nanosilica without functionalization, since they killed almost all the bacteria after the 24 h incubation.**

Table 3. The antibacterial activity against *Staphylococcus aureus* in SiO₂-75 and BF-85 samples.

Sample	mg/ml	t=0 (cfu average/ml)	t=24 (cfu average/ml)	R (log) vs <i>S. aureus</i>	R (log) vs SiO ₂
<i>S. Aureus</i>		1,6 x 10 ⁵	3,3 x 10 ⁶		
SiO ₂	1	1,6 x 10 ⁵	9,8 x 10 ³	2,53	
BF-SiO ₂	1	1,6 x 10 ⁵	3	6,04	3,51

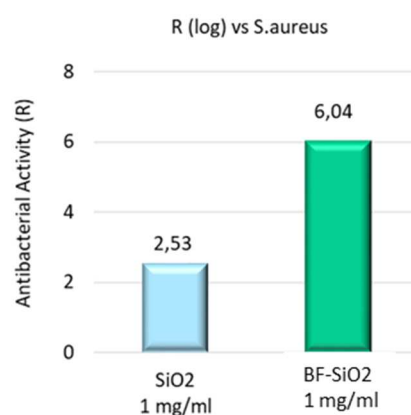


Figure 25. The antibacterial activity against *Staphylococcus aureus* in SiO₂-75 and BF-85 samples.

5.1.2 Incorporation of permanent biocide particles into PUR matrix

The biocide nanoparticles have been incorporated into the polyurethane formulations prepared by FUNDITEC, which were 2-component (2K). More precisely, the biocide nanoparticles (BF-85) were added to one of the components of the formulation in different concentrations (1, 10 and 25% wt.) and on the other hand, a control system without nanoparticles was prepared.

Each synthesized polyurethane matrix was applied following the curing condition established by FUNDITEC, 60°C for 4h on two types of substrates that were sent by CANOE: (i) uncoated composite and (ii) the same composite covered with gelcoat.



Table 4. Prepared coatings on the different composites.

Ref.	Substrate	Nanoparticles		Curing
		Ref.	% wt.	
CPUR_0	Uncoated composite	-	0	60°C 4h
CPUR_1	Uncoated composite	BF-85	1	60°C 4h
CPUR_10	Uncoated composite	BF-85	10	60°C 4h
CPUR_25	Uncoated composite	BF-85	25	60°C 4h
CGPUR_0	Composite + gelcoat	-	0	60°C 4h
CGPUR_1	Composite + gelcoat	BF-85	1	60°C 4h
CGPUR_10	Composite + gelcoat	BF-85	10	60°C 4h
CGPUR_25	Composite + gelcoat	BF-85	25	60°C 4h

Figure 26 shows the appearance of the polyurethane coatings on uncovered composites. It was observed that the coatings were transparent and nanoparticle dispersion was more uniform when adding 25% rather than only 1% of nanoparticles. The latter presented sporadic aggregates along the surface.

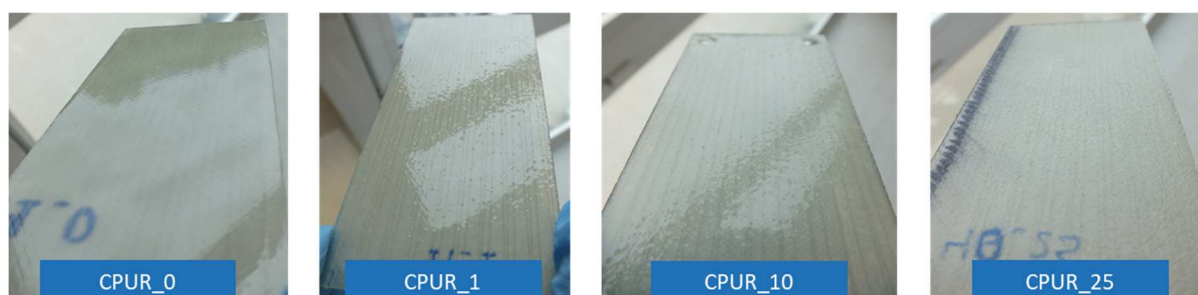


Figure 26. Appearance of Funditec polyurethane coatings on uncovered composites

5.1.3 Test Results

The resulting coatings described above were studied using different analytical techniques. The characterization was focused to the following features:

- Surface roughness: ISO 4288 “Geometrical Product Specifications (GPS) - Surface texture: Profile method - Rules and procedures for the assessment of surface texture”.
- Contact angle: Digidrop Contact Angle Meter (GBX Instruments).
- Coating adhesion: ISO 2409 “Paints and varnishes — Cross-cut test”.
- Hardness: ASTM 3363-05 “Standard Test Method for Film Hardness by Pencil Test”.
- Exposure in real environment at the port of Pasaia: ASTM D6990-05 “Standard Practice for Evaluating Biofouling Resistance and Physical Performance of Marine Coating Systems”.

5.1.3.1 Roughness and contact angle

Table 5 shows the results of roughness on all prepared samples and the contact angle measurements. As expected, the superficial roughness increased as the concentration of nanoparticles increased and



the composites covered with gelcoat presented higher roughness than uncovered composites.

Regarding contact angle measurements, it was observed that values did not vary with the concentration of nanoparticles added. However, contact angle resulted to be high, being highly close to hydrophobic (88°).

Table 5. *Roughness and contact angle measurements of synthetic polyurethane*

Ref.	Substrate	Nanoparticles BF85 (%)	Roughness (Ra, μm)	Contact angle water (°)
CPUR_0	Uncoated composite	0	0,06	88
CPUR_1	Uncoated composite	1	0,1	88
CPUR_10	Uncoated composite	10	2,5	88
CPUR_25	Uncoated composite	25	9,7	85
CGPUR_0	Composite + gelcoat	0	0,01	
CGPUR_1	Composite + gelcoat	1	0,4	
CGPUR_10	Composite + gelcoat	10	3,4	
CGPUR_25	Composite + gelcoat	25	10,3	

5.1.3.2 Adhesion to the substrate and hardness by pencil

Table 6 summarizes the results of adhesion test and hardness by pencil performed. The results are on a scale 0 to 5, with 0 being the best results. In all cases, the coatings showed good adhesion to the substrate, excepting when high concentrations of nanoparticles (10-25%) were present in the coatings. Such poor adherence can be attributed to use of mild curing conditions (60°C, 4h) and therefore, an incomplete cured of the matrix. On the other hand, increasing concentration of nanoparticles in the coating did not vary the hardness by pencil measurements.

Table 6. *Adhesion and hardness of commercial and synthetic polyurethane*

Ref.	Substrate	Nanoparticles BF-85 (%)	Adhesion	Scratch hardness
CPUR_0	Uncoated composite	0	0	B
CPUR_1	Uncoated composite	1	0	F
CPUR_10	Uncoated composite	10	4	B
CPUR_25	Uncoated composite	25	1	B
CGPUR_0	Composite + gelcoat	0	0	HB
CGPUR_1	Composite + gelcoat	1	0	B
CGPUR_10	Composite + gelcoat	10	1	B
CGPUR_25	Composite + gelcoat	25	5	B

5.1.3.3 Biofouling resistant by exposure on sea immersion conditions (Pasaia's Port).

The main objective of the NEMMO project consists in reducing the hydrodynamic resistance of marine surfaces due to biofouling build-up. For such reason, these coatings have been evaluated at the Pasaia's port on sea immersion conditions. Biofouling is the accumulation of microorganisms, plants,



algae, on wetted surfaces. Biofouling is divided into microfouling (biofilm formation and bacterial adhesion) and macrofouling (attachment of larger organisms).

Figure 27 and Figure 28 show the visual inspections that were carried out over a time course of 60, 120 and 150 days. In all samples, microfouling growth was observed and identified as barnacles. However, in the case of polyurethane coatings on uncovered composite, the density of barnacles adhered on the surface was greatly reduced during exposure. This effect was more easily observable after 150 days of exposure (Figure 27). However, the quantity of fouling attached did not vary with the concentration of nanoparticles added. On the other hand, in the case of polyurethane coatings on composite covered with gelcoat, it was observed a high density of barnacles attached on surface in all samples (Figure 28).

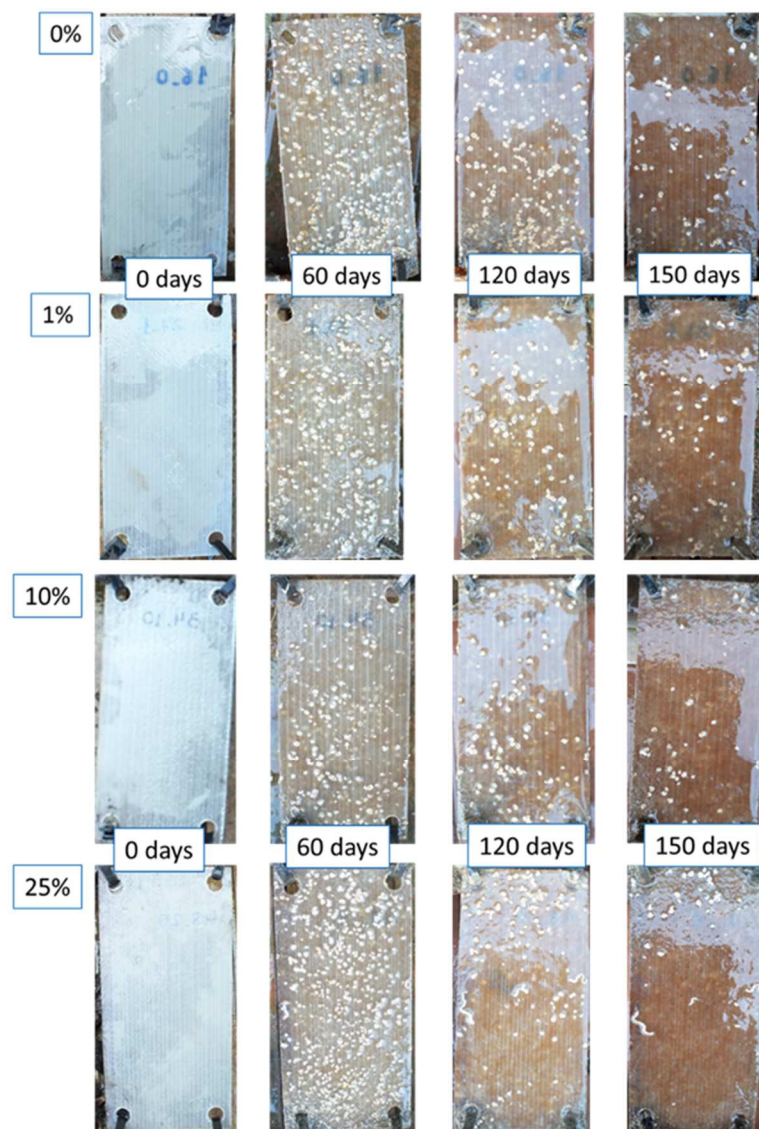


Figure 27. Aspect of polyurethane with 0, 1, 10 and 25 % of nanoparticles on uncovered composite after 0, 60, 120 and 150 days.



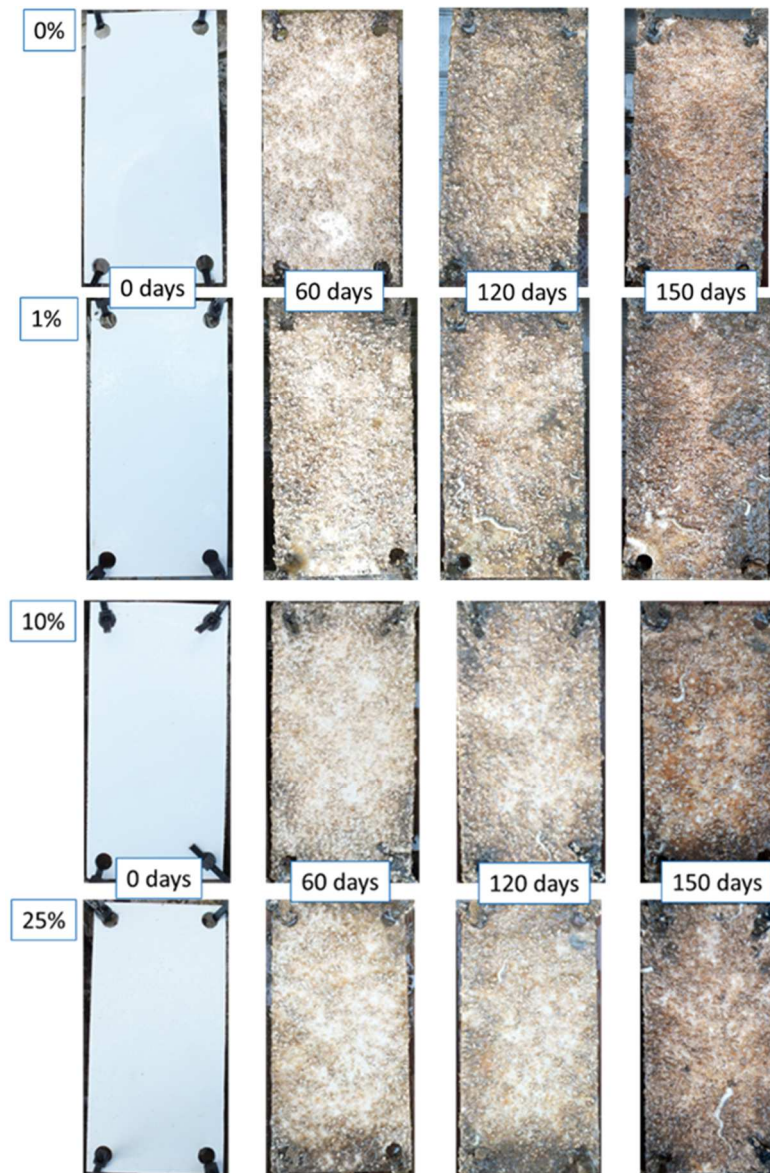


Figure 28. Aspect of polyurethane with 0, 1, 10 and 25% of nanoparticles on composite covered with gelcoat after 0, 60, 120 and 150 days.

After 5 months of exposure to sea immersion condition, biofouling resistance was evaluated according to standard ASTM D6990-05 “Standard Practice for Evaluating Biofouling Resistance and Physical Performance of Marine Coating Systems”. The surface of test panels was cleaned using low-pressure water at a controlled distance and the percentage of biofouling attached directly to the coating system was evaluated.

In the case of polyurethane coatings on uncovered composite, although the microfouling growth was least than on composite covered with gelcoat, degradation and colour loss of composite was observed (Figure 29). On the other hand, in the case of polyurethane on composite covered with gelcoat, it was observed that the density of barnacle attached on the surface was slightly reduced on coating systems



with 10-25% biocide nanoparticles. In particular, the percentage cover of fouling was reduced 20% compared to control system without nanoparticles (Figure 30).

Table 7. Percentage of biofouling attached on polyurethane surface with and without nanoparticles incorporated.

Ref.	Substrate	Nanoparticles BF-85 (%)	% Fouling
CPUR_0	Uncoated composite	0	1%
CPUR_1	Uncoated composite	1	3%
CPUR_10	Uncoated composite	10	3%
CPUR_25	Uncoated composite	25	3%
CGPUR_0	Composite + gelcoat	0	90%
CGPUR_1	Composite + gelcoat	1	80%
CGPUR_10	Composite + gelcoat	10	70%
CGPUR_25	Composite + gelcoat	25	70%

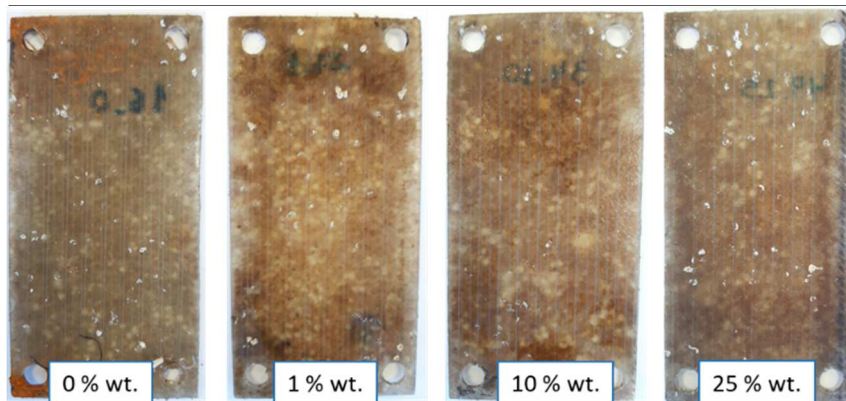


Figure 29. Aspect of polyurethane with 0, 1, 10 and 25 % of nanoparticles on uncovered composites after being wetted/cleaned using low-pressure water.

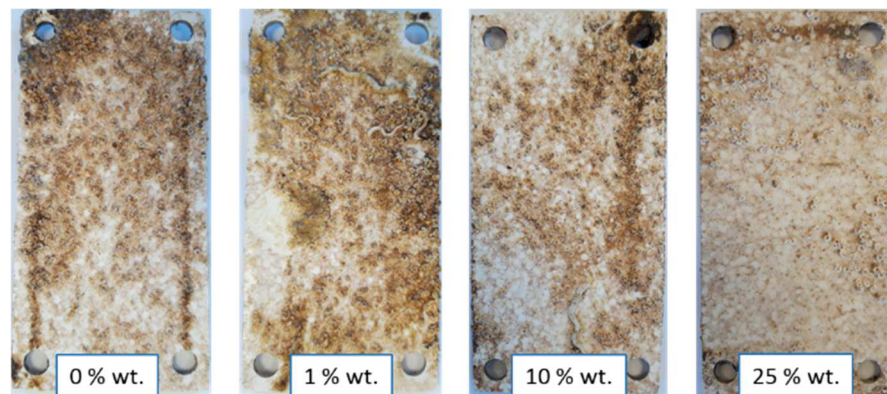


Figure 30. Aspect of polyurethane with 0, 1, 10 and 25 % of nanoparticles on composite covered with gelcoat after being wetted/cleaned using low-pressure water.

5.1.4 Conclusions

- Stable non-functionalised/pristine silica colloidal dispersions have been obtained by sol-gel method which have been functionalized with biocide moieties in two-step method, maintaining the stability. Z Potential and DLS measurements indicated stable dispersions.
- Full characterisation of these nanoparticles has been carried out: DLS and TEM show particle sizes of 85 nm.
- Functionalized nanoparticles have showed higher antibacterial activity against *S. aureus* than non-functionalised nanosilica.
- The incorporation of biocide nanoparticles in polyurethane formulations was accomplished. The addition of high quantities of nanoparticles (25 %) formed coatings with higher homogeneity, higher roughness but lower adherence to the substrate.
- The assessment accomplished after cleaning the samples according to the standard, ASTM D6990-05 revealed that the density of barnacles attached on polyurethane coatings on uncovered composite was greatly reduced during exposure on sea immersion conditions. However, degradation and colour loss of composite was observed.
- The assessment accomplished after cleaning the samples according to the standard, ASTM D6990-05 revealed that the density of barnacle attached on polyurethane on composite covered with gelcoat was slightly reduced on coating systems with 10-25% biocide nanoparticles. In particular, the percentage cover of fouling was reduced 20% compared to control system without nanoparticles.



5.2 Development of highly crosslinked PUD containing cationic co-polymers and particles for cavitation and antifouling resistance. *Task 3.3.2. FUNDITEC.*

5.2.1 Introduction

Task 3.3.2 focuses on the development of non-leaching anti-fouling coatings with permanent cavitation resistance through the design and synthesis of polymers bearing different functionalities within its chemical backbone.

Two different synthetic approaches have been considered based on highly cross-linked elastomeric polyurethanes:

- Synthesis of two components (2K) polyurethanes with fluorinated moieties in the polymer backbone (FPU) to decrease the surface energy of the coating and prevent the attachment of microorganisms.
- Synthesis of one component (1K) polyurethane dispersions (PUD) with cationic chemical groups in the structure, acting as non-leaching permanent biocide interfering in the first colonization stages of microorganisms.

During this research, different materials and procedures for the synthesis of polymeric coatings have been tested, including the incorporation of nanoparticles to improve resistance to erosion and fouling. In addition, the behaviour of the resulting coatings applied on composite material have been evaluated by a thorough characterization and those with the best performing properties have been selected as a topcoat solution for tidal turbine composite blades.

5.2.2 2K fluorinated polyurethanes

5.2.2.1 Synthesis

The formulation of this type of polyurethane comprises a polyisocyanate as a curing agent (Component A) and a polyol (Component B) that are mixed and react to form a polymeric coating crosslinked by urethane bonds.

The synthesis of component A was the subject of the development and it was produced in a two-step procedure. Briefly, the first step consists in the reaction of a polyol with an excess of a diisocyanate to yield an NCO-terminated polyurethane prepolymer. In the second step, some of the NCO groups are blocked with either a fluorinated monomer or an acrylated monomer, yielding different properties in the final polyurethane coating. Various polyols, and fluorinated and acrylated monomers were tested to obtain functionalized polyisocyanates with different chemical structure.

Based on reactivity of monomers, reproducibility and scalability of the reactions, one hyperbranched polyol was selected to synthesize the NCO-terminated prepolymer on the first step (hereinafter sample 1001). With the same criteria, two compounds were selected in the second step to obtain fluorinated polyisocyanate (coded as 2001B) and acrylated polyisocyanate (3002) (Figure 31).





Figure 31. Acrylated (3002) and fluorinated (2001B) polyisocyanates synthesised by FUNDITEC.

5.2.2.2 Formulation of coatings and application on glass substrates

Depending on the functional group of the polyisocyanate, two types of coatings were formulated:

- Type I (hereinafter referred to as Coating 13): Fluorinated polyisocyanate 2001B (component A) and commercial acrylic polyol (component B).
- Type II (Coating 15): Acrylated polyisocyanate 3002 (component A) and commercial fluorinated polyol (component B).

Component A and component B were mixed with an NCO:OH ratio of 1:1. In order to obtain a uniform and smooth surface coating with good adhesion and hardness, several formulations of 2K FPU were tested based on:

- adjustment of the concentration of component A in an appropriate solvent,
- use of additives (wetting, anti-crater or antifoaming agents) and
- optimization of the curing conditions (type and amount of catalyst, temperature, time and UV irradiation).

The formulations were applied onto glass substrates with a wet film thickness of 100 μm using a K-hand coater.

The optimized coatings were characterized after one week at ambient conditions. Hardness and adhesion were measured according to the standards ASTM D3363 and ASTM D3359, respectively. Samples were analyzed by differential scanning calorimetry (DSC) to determine glass transition temperature (T_g): heating from room temperature to 100°C, cooling to -70°C and heating again to 150°C at a rate of 20°C/min. Table 8 summarizes the composition, the curing conditions, and the results of the physical properties of the coatings.

Table 8. Composition, curing conditions and physical properties of 2K FPU coatings applied on glass substrates.

Code	Composition	Curing	Hardness	Adhesion	T_g (°C)
Coating 13	T catalyst Additives	100°C 2h + RT 1week	H	3B	23,8
Coating 15	T catalyst UV catalyst Additives	100°C 1h + UV 5min	4H	2B	28,8

FT-IR analysis (Figure 32) confirmed both the urethane formation and the crosslinking of acrylates by the disappearance of absorption bands corresponding to either isocyanate or acrylated groups.



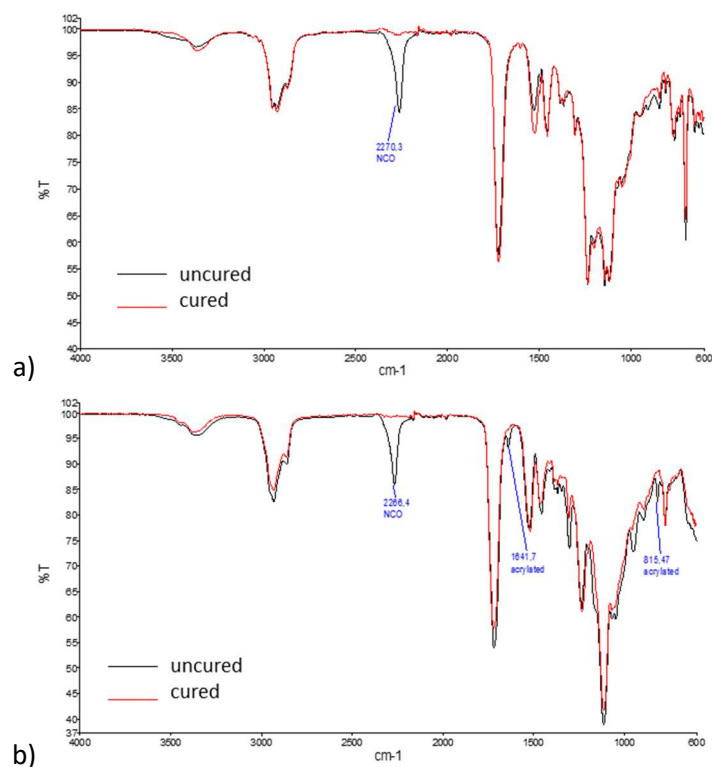


Figure 32. FT-IR spectra of cured and uncured 2K fluorinated polyurethanes: a) Coating 13 and b) Coating15.

5.2.3 1K cationic polyurethane dispersions

5.2.3.1 Synthesis

The second approach was the synthesis of water based one-component polyurethane dispersions (PUD) with cationic chemical groups in the polymer backbone.

Several aqueous cationic PUDs were synthesized by the ketone method which is based on the formation of a polymer through urethane bonds by the coupling reaction of a diisocyanate, polyol and a tertiary amine diol followed by treatment with an acid to form the quaternary ammonium group and dispersion in water at high speed.

Different reaction parameters such as mass of reactants, NCO/OH ratio and solid content were tested. Based on the stability of the dispersion over time, polyurethane dispersion coded as PUD5 (Figure 33) with an NCO/OH ratio of 1.14 and a solid content of 32.5% was selected.



Figure 33. Water based polyurethane dispersion PUD5 synthesised by FUNDITEC.



5.2.3.2 Formulation of coatings and application on glass substrates

In order to obtain a uniform and smooth surface coating with good adhesion and hardness, several formulations of PUD5 were tested based on:

- i) use of additives (wetting, anti-crater or antifoaming agents) and
- ii) optimization of the curing conditions (type and amount of catalyst, time and UV irradiation).

The formulations were applied onto glass substrates with a wet film thickness of 100 μm using a K-hand coater. The optimized coating was characterized after one week at ambient conditions. Hardness, adhesion and glass transition temperature were determined as described before. Table 9 summarizes the composition, the curing conditions, and the results of the physical properties of the coating.

Table 9. Composition, curing conditions and physical properties of PUD5 coating applied on glass substrate.

Code	Composition	Curing	Hardness	Adhesion	Tg ($^{\circ}\text{C}$)
Coating PUD5	UV catalyst Additives	RT overnight + UV 10min	4H	4B	44,6

FT-IR analysis (Figure 34) confirmed the crosslinking of acrylate groups by the disappearance of the absorption bands corresponding to the acrylated groups.

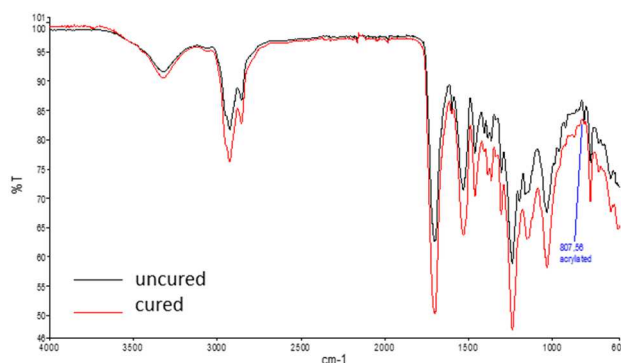


Figure 34. FT-IR spectra of cured and uncured polyurethane coating PUD5.

5.2.4 Incorporation of nanoparticles into the polyurethane matrix

5.2.4.1 Incorporation of carbon nano-complexes

Improvement of wear and impact resistance and enhancement of the barrier properties of the turbine blades, to prevent saline water permeation, play an important role. To increase mentioned parameters, it has been proposed the reinforcement of polyurethane coatings with carbon nano-complexes containing SP1 protein and different nanoparticles (NP) such as: MWCNT, SWCNT, 2 types of graphene and CB.

To enable dispersion of these complexes in polyurethane, SP Nano prepared different carbon nanoparticles dispersions/pastes using its proprietary technology, SP1, an engineered protein with high affinity towards graphitic surfaces, e.g., carbon nanotubes (CNT), graphene, carbon black (CB)



and other carbon nanoparticles (CNP). Table 10 shows the samples of carbon nano-complexes prepared by SP Nano and received at FUNDITEC to be incorporated into the polyurethane matrixes.

Table 10. Carbon nano-complexes prepared by SPNano.

Sample	NP/SP1 complex	NP/SP1 ratio	NP/Latex ratio	Total sample weight (g)	% CNP	Sample type
CNP1	CB/SP1	25		9,9	32,3%	Paste1
CNP2	MWCNT/SP1	10		19,4	9,8%	Paste1
CNP3	CB/SP1/Latex	25	4	10,0	26%	Paste1
CNP4	MWCNT/SP1/Latex	10	4	19,4	14,9%	Paste1
CNP5	CB/SP1	25		2,84	86,7%	Powder
CNP6	Graphene1/SP1	28		0,38	87,5%	Powder
CNP7	Graphene2/SP1	16		0,52	80,0%	Powder
CNP8	MWCNT/SP1	10		0,60	69,7%	Powder
CNP9	SWCNT/SP1	1		0,17	17,4%	Powder
CNP10	CB/SP1	25		15,5	22,6%	Paste2
CNP11	MWCNT/SP1	11		24,1	2,5%	Paste2
CNP12	SWCNT/SP1	1		19,1	0,8%	Paste2

Out of the twelve samples received, eight samples (1, 2, 5, 7, 8, 10, 11 and 12) were selected for the dispersion tests, based on type (powder, paste, latex), % NP content, and amount available of material. Therefore, fourteen dispersions were prepared by mixing the nano-complexes with component B of solvent-based resins or with the water-based polyurethane dispersion (PUD) using Ultra Turrax with a speed range of 10k rpm, during 10 min and with addition of 0,1% carbon NP (Table 11, Figure 35).

Table 11. Dispersion tests performed with carbon nano-complexes. *+ 6min

Sample	Resin	Complex Sample	Type NP	Sample type
I	Comp. B Coating15	CNP1	CB	Solvent paste1
II	Comp. B Coating15	CNP10	CB	Solvent paste2
III	Comp. B Coating15	CNP2	MWCNT	Solvent paste1
IV	Comp. B Coating15	CNP11	MWCNT	Solvent paste2
V	Comp. B Coating15*	CNP5	CB	Dry powder
VI	Comp. B Coating15	CNP12	SWCNT	Solvent paste2
VII	PUD5	CNP5	CB	Dry powder
VIII	PUD5	CNP8	MWCNT	Dry powder
IX	PUD5bis	CNP5	CB	Dry powder
X	PUD5	CNP7	Graphene2	Dry powder
XI	Comp. B Coating13	CNP1	CB	Solvent paste1
XII	Comp. B Coating13	CNP10	CB	Solvent paste2



XIII	Comp. B Coating13	CNP11	MWCNT	Solvent paste2
XIV	Comp. B Coating13	CNP5	CB	Dry powder

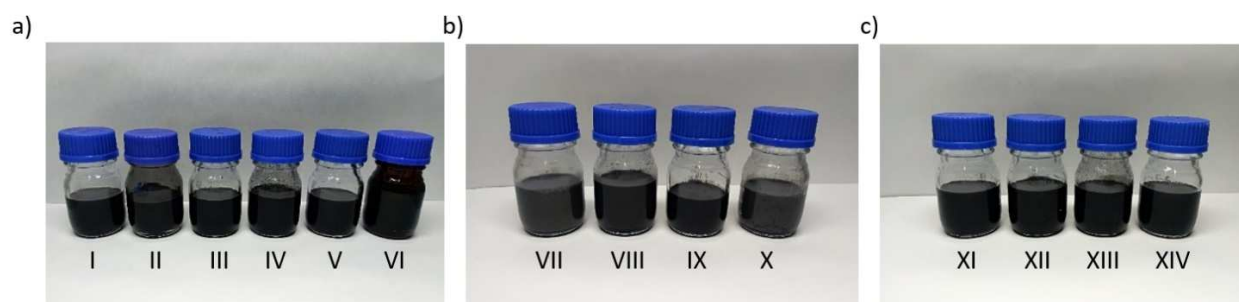


Figure 35. Carbon NP dispersions: a) based on component B of Coating15, samples I-VI, b) based on PUD, samples VII-X, c) based on component B of Coating13, samples XI-XIV.

During the trials, we could analyse and compare the dispersibility of various types of NPs (CB, MWCNT, graphene) and samples (powder or paste) in two solvent-based resins and one water-based dispersion.

We observed many problems to achieve proper dispersion of carbon NP: sedimentation, agglomeration, and non-dispersed particles, especially in case of MWCNT as solvent paste2 (Figure 36).



Figure 36. Problems observed during dispersion tests: sedimentation and non-dispersed particles.

The best results were obtained using CB/SP1 type of nano-complexes in all cases. Regarding the sample type, paste2 gave better results than powder or paste1 for the solvent resin, affording dispersions stable over time. For those reasons, we selected the CB/SP1 paste2 for the solvent-based coatings (Coating13 + CNP10 and Coating15 + CNP10) and CB/SP1 as powder for the water-based polyurethane (PUD5 + CNP5).

In addition to Ultra Turrax, Ultrasonication (13mm diameter sonication probe, 60% amplitude and 5min treatment) was also tested as dispersion method, obtaining similar results. The best results for the dispersion of nanocomplexes in Lumiflon LF910 using sonication were obtained for CB/SP1 paste2.

Formulation of coatings was carried out according to the selected nano-complex dispersions (with 0,1% of carbon NP in respect to the total coating), applied on glass substrates (Figure 37) with a wet film thickness of 100 µm using a K-hand coater and cured with the previously established conditions



for each type of coating. The coatings demonstrate that CB/SP1 is homogenously dispersed in the different polyurethanes.

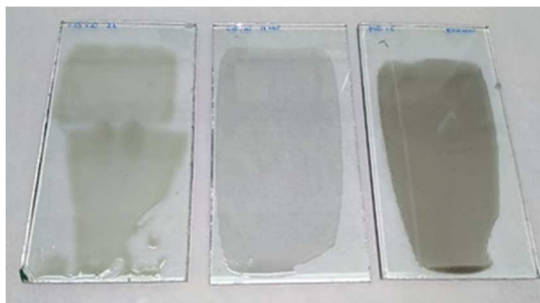


Figure 37. Polyurethane coatings applied on glass: Coating 13+CNP10, Coating 15+CNP10 and PUD5+CNP5 (from left to right).

Comparative analysis of the mechanical properties of the coatings applied on glass substrates (Table 12) showed that the adhesion values remained constant after adding carbon NP for all type of coatings. The same can be observed with the hardness values. However, there is a slight improvement (from 4H to 5H) in case of PUD reinforced with CB/SP1 coating. The hardness of Coating 13 does not increase with the addition of carbon NP and its value remains low (H). Therefore, Coating 15+CNP10 and PUD5+CNP5 were selected to be applied on gel-coated composite substrate supplied by CANOE.

Table 12. Comparative results of hardness and adhesion of the coatings with carbon NP.

Characterization	Coating 13	Coating 13 +CNP10	Coating 15	Coating 15 +CNP10	PUD5	PUD5 +CNP5
Adhesion	5B	5B	5B	5B	5B	5B
Hardness	H	H	4H	4H	4H	5H

5.2.4.2 Incorporation of functionalised silica nanoparticles

Functionalised silica nanoparticles with biocide activity (sample BF_85) were received from TECNALIA and were incorporated into polyurethane matrix to test cavitation erosion resistance and antifouling properties on composite substrate.

Two dispersions were prepared by mixing the silica nanoparticles with component B of Coating 15 or with the water-based polyurethane dispersion PUD5 using Ultra Turrax with a speed range of 10k rpm for 5 min. The amount of SiO₂ NP was established at 1% by weight of the coating after drying.

Both samples showed good dispersion of silica nanoparticles, no sedimentation and stability over time (Figure 38). The formulation and application of these coatings on gel-coated composite substrate is detailed in the next section.



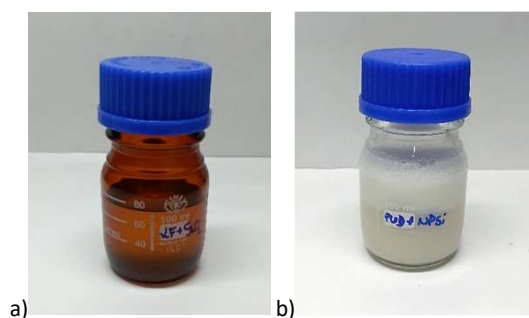


Figure 38. Silica NP dispersions: a) with component B of Coating15 and b) with PUD5.

5.2.5 Application of coatings on composite substrate

Selected coatings developed by FUNDITEC as well as commercial topcoat products were applied on gel-coated composite substrate supplied by CANOE following the scheme illustrated in Figure 39.

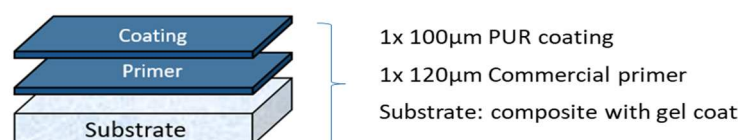


Figure 39. Scheme of the different layers deposited on composite substrate provided by CANOE.

The substrate was first coated with a commercial primer with a wet film thickness of 120 µm using a K-hand coater and dried for 24h at room temperature. Subsequently, the coatings by FUNDITEC and the commercial ones were formulated according to Table 13 and applied with a wet film thickness of 100 µm on the primer-coated composite. The resulting films were cured with the previously established parameters for each type of coating (Table 13). Images of the coated composite substrates with FUNDITEC's polyurethanes and commercial coatings are shown in Figure 40.

Table 13. Final coating formulations and curing conditions.

Code	Formulation	Curing
Primer	Commercial primer	RT 24h
Commercial White	Commercial topcoat	RT 24h
Commercial Black	Commercial topcoat	RT 24h
Coating 13	Component A + B: Fluorinated polyisocyanate (2001B) + Acrylic polyol T catalyst Additives	100°C 2h + RT 1week
Coating 15	Component A + B: Acrylated polyisocyanate (3002) + Fluorinated polyol T catalyst UV catalyst Additives	100°C 1h + UV 5min
Coating 15 + CNP10	+ 0.1% CNP10	
Coating 15 + SiO₂	+ 1% SiO ₂	



PUD5	1 component: PUD5 UV catalyst Additives	RT overnight + UV 10min
PUD5 + CNP5	+ 0.1% CNP5	
PUD5 + SiO₂	+ 1% SiO ₂	

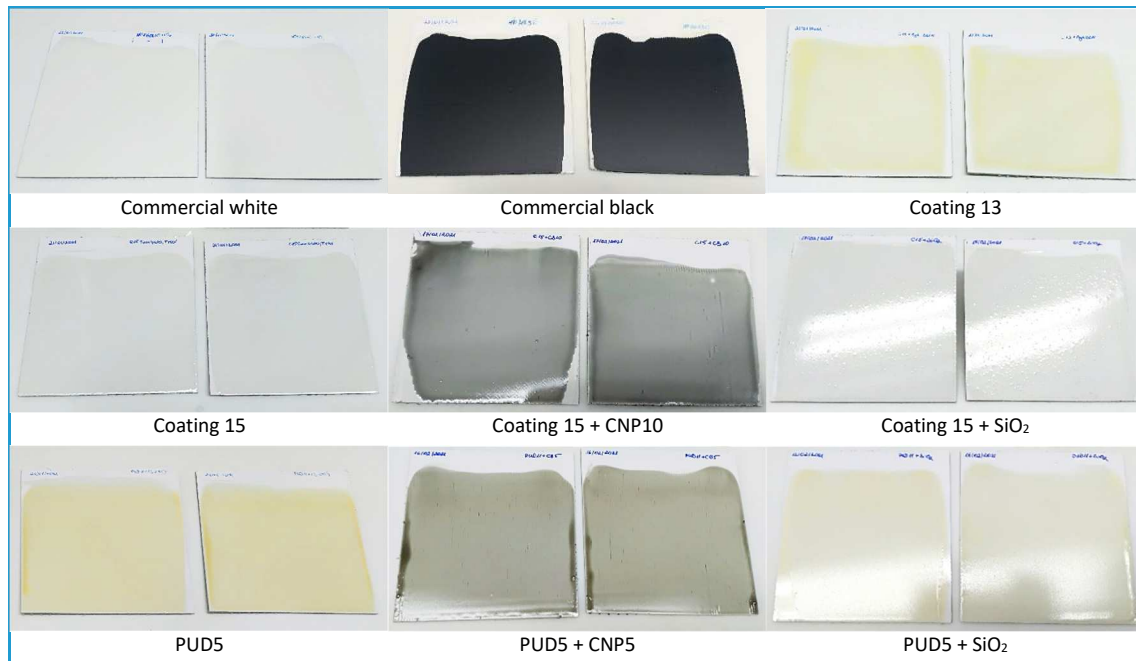


Figure 40. FUNDITEC's polyurethane with and without reinforcement of SP Nano's CB/SP1 nano-complex and commercial coatings applied on composite substrate.

5.2.6 Characterisation of coatings

5.2.6.1 Mechanical properties

The coatings applied on composite substrate were characterized after one week at ambient conditions. Hardness and adhesion were measured according to the standards ASTM D3363 and ASTM D3359, respectively. Table 14 shows the results of the mechanical characterisation.

Table 14. Hardness and adhesion values of the coatings applied on composite substrates.

Code	Adhesion	Hardness
Commercial White	0B	B
Commercial Black	0B	B
Coating 13	5B	H
Coating 15	5B	4H
Coating 15 + CNP10	5B	4H
Coating 15 + SiO₂	5B	4H
PUD5	5B	5H



PUD5 + CNP5	5B	5H
PUD5 + SiO₂	5B	5H

The new developed coatings showed all of them good adhesion on the composite substrate, and a remarkable different with the commercial ones. Results on hardness were also good for both the solvent-based coating 15 and water-based PUD5 although slightly different.

5.2.6.2 Cavitation erosion tests

The final stage of the development of polyurethane coatings for tidal turbine composite blades focuses on the study of their resistance to cavitation erosion.

Tests were performed according to ASTM G32 “Standard Test Method for Cavitation Erosion Using Vibratory Apparatus”. Although the mechanism for generating fluid cavitation in this method differs from that occurring in flowing systems, the nature of the material damage mechanism is believed to be basically similar. The method therefore offers a small-scale test that can be used to compare the cavitation erosion resistance of different materials¹.

A schematic setup of cavitation erosion test is shown in Figure 41. Sonics Vibra-cell VCX 750 ultrasonic processor was used with a vibratory amplitude and output frequency of 50 μm and 20 kHz, respectively. The tests were conducted in indirect cavitation mode in which the sample (2x2 cm coated composite) was placed 0.5 mm from the sonotrode with a tip diameter of 13 mm. Distilled water was chosen as the immersion liquid and temperature was maintained stable by circulating fresh water in the cooling bath.

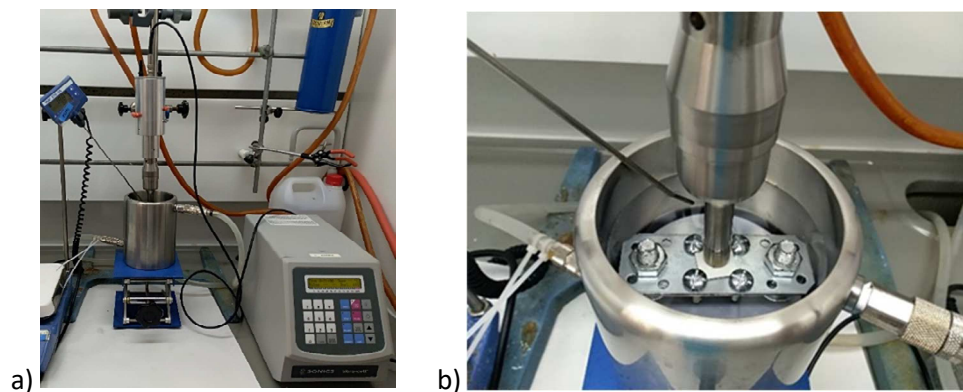


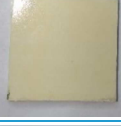
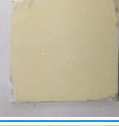
Figure 41. a) Setup of cavitation erosion test and b) Close-up of the sample holder.

Cavitation tests with a total exposure time of 5 minutes were performed twice for each type of material, with time intervals of 1 minute for visual inspection of the coating surface (Table 15).

¹ <https://www.astm.org/Standards/G32>



Table 15. Visual evaluation of coating surface after cavitation erosion test.

Code	0 min	1 min	2 min	3 min	4 min	5 min
Commercial topcoat white						
Commercial topcoat black						
Coating 13						
Coating 15						
Coating 15 CNP						
Coating 15 SiO ₂						
PUD5						
PUD5 CNP						
PUD5 SiO ₂						

After the cavitation tests, samples were dried, and then weighed. The mass loss of the coating, calculated as the percentage difference between the initial and final state, are shown in Table 16.



Table 16. Results of mass loss after cavitation erosion test.

Code	% mass loss
Commercial topcoat white	2,0286
Commercial topcoat black	2,5881
Coating 13	0,6385
Coating 15	0,0187
Coating 15 CNP	0,0350
Coating 15 SiO ₂	0,0813
Coating PUD	0,0175
Coating PUD CNP	0,1576
Coating PUD SiO ₂	0,0415

As it can be seen from the results, the developed coatings show better resistance to erosion than commercial ones. Almost no sample wear is visible during the cavitation test for Coating 15 and PUD5 (about 0,02% mass loss) in contrast to Coating 13 which shows an eroded surface and a 0.64% mass loss. Incorporation of carbon and silica nanoparticles into the PUR matrix has no significant effect on the resistance to cavitation erosion. Therefore, Coating15 and PUD5 were selected as the best topcoat solutions for tidal turbine composite blades. The selection of the final coating and the effect of carbon and silica nanoparticles will be assessed based on the antifouling tests performed by DCU and TECNALIA.

5.2.7 Conclusions

- Three different polyisocyanates (component A) with a dendritic aliphatic polyester core and fluorinated or acrylated functionalities were successfully synthesized.
- 2K fluorinated polyurethanes were formulated with the synthesized component A and applied on glass and composite substrate. From the characterization of the coatings, two types of formulations were selected (Coating 13 and Coating 15). They showed good mechanical properties, glass transition temperatures around 20-25°C and different hydrophobicity behaviour that can either prevent the biofouling or improve the release of settled biofouling by the water flow.
- Several aqueous cationic PUDs were synthesized based on the formation of a polymer with urethane bonds through the reaction of a diisocyanate, polyols and a tertiary amine diol followed by treatment with an acid and dispersion in water at high speed, where based on the stability of the dispersion over time, the polyurethane dispersion PUD5 with an NCO/OH ratio of 1.14 and a solid content of 32.5% was selected.
- Both types of coatings (solvent-based and water-based) showed good hardness and adhesion properties with values around 5B and 4H respectively.
- An in-depth study was carried out to obtain the best conditions for the preparation of stable dispersions of nano-complexes, provided by SPNANO with different carbons (graphene, CB, CNTs) and the SP1 protein and the two types of components in FUDNITEC's formulations.



- The functionalized silica nanoparticles prepared by TECNALIA and the carbon nanocomplexes prepared by SPNANO were added to the formulation of the two types of coatings developed by FUNDITEC (Coating 15 and PUD5) and the properties of the resulting coatings also tested.
- Mechanical properties (adhesion and hardness) seem not to be improved neither diminished upon the inclusion of any of the two types of nanoparticles.
- Regarding erosion resistance, it seems that the developed coatings show better resistance to erosion than commercial ones. Coating 15 and PUD5 performed the best (about 0,02% mass loss) in contrast to Coating 13 which shows an eroded surface and a 0.64% mass loss. Incorporation of carbon and silica nanoparticles into the PUR matrixes has no significant effect on the resistance to cavitation erosion.
- Coating15 and PUD5 were selected as the best topcoat solutions for tidal turbine composite blades waiting for the results of antifouling tests performed by DCU and TECNALIA.



References

- [1] K. A. Dafforn, J. A. Lewis, and E. L. Johnston, "Antifouling strategies: History and regulation, ecological impacts and mitigation," *Mar. Pollut. Bull.*, vol. 62, no. 3, pp. 453–465, 2011.
- [2] C. Richards, N. O. Connor, D. Jose, A. Barrett, and F. Regan, "Selection and optimization of protein and carbohydrate assays for the characterization of marine biofouling," *Anal. Methods*, vol. 12, no. 17, pp. 2228–2236, 2020.
- [3] S. Durr and J. C. Thomason, *Biofouling*. 2009.
- [4] M. H. Andersson, M. Berggren, D. Wilhelmsson, and M. C. Öhman, "Epibenthic colonization of concrete and steel pilings in a cold-temperate embayment: A field experiment," *Helgol. Mar. Res.*, vol. 63, no. 3, pp. 249–260, 2009.
- [5] J. E. Gittens, T. J. Smith, R. Suleiman, and R. Akid, "Current and emerging environmentally-friendly systems for fouling control in the marine environment," *Biotechnol. Adv.*, vol. 31, no. 8, pp. 1738–1753, 2013.
- [6] R. J. Crawford, H. K. Webb, V. K. Truong, J. Hasan, and E. P. Ivanova, "Surface topographical factors influencing bacterial attachment," *Adv. Colloid Interface Sci.*, vol. 179–182, no. 1, pp. 142–149, 2012.
- [7] K. Anselme, P. Davidson, A. M. Popa, M. Giazzon, M. Liley, and L. Ploux, "The interaction of cells and bacteria with surfaces structured at the nanometre scale," *Acta Biomater.*, vol. 6, no. 10, pp. 3824–3846, 2010.
- [8] M. J. Dalby, N. Gadegaard, and R. O. C. Oreffo, "Harnessing nanotopography and integrin-matrix interactions to influence stem cell fate," *Nat. Mater.*, vol. 13, no. 6, pp. 558–569, 2014.
- [9] L. D. Chambers, K. R. Stokes, F. C. Walsh, and R. J. K. Wood, "Modern approaches to marine antifouling coatings," *Surf. Coatings Technol.*, vol. 201, no. 6, pp. 3642–3652, 2006.
- [10] L. C. Hsu, J. Fang, D. a Borca-Tasciuc, R. W. Worobo, and C. I. Moraru, "Effect of micro- and nanoscale topography on the adhesion of bacterial cells to solid surfaces.," *Appl. Environ. Microbiol.*, vol. 79, no. 8, pp. 2703–7212, 2013.
- [11] J. F. Schumacher, C. J. Long, M. E. Callow, J. a. Finlay, J. a. Callow, and A. B. Brennan, "Engineered nanoforce gradients for inhibition of settlement (attachment) of swimming algal spores," *Langmuir*, vol. 24, no. 9, pp. 4931–4937, 2008.
- [12] A. V. Bers and M. Wahl, "The influence of natural surface microtopographies on fouling," *Biofouling*, vol. 20, no. 1, pp. 43–51, 2004.
- [13] M. E. Callow *et al.*, "Microtopographic Cues for Settlement of Zoospores of the Green Fouling Alga *Enteromorpha*," *Biofouling*, vol. 18, no. 3, pp. 237–245, 2002.
- [14] A. J. Scardino, E. Harvey, and R. De Nys, "Testing attachment point theory : diatom attachment on microtextured polyimide biomimics," *Biofouling*, vol. 22, no. 1, pp. 55–60, 2006.
- [15] M. Lorenzetti *et al.*, "The influence of surface modification on bacterial adhesion to titanium-



- based substrates,” *ACS Appl. Mater. Interfaces*, vol. 7, no. 3, pp. 1644–1651, 2015.
- [16] C. Richards, A. Slaimi, N. E. O’Connor, A. Barrett, S. Kwiatkowska, and F. Regan, “Bio-inspired surface texture modification as a viable feature of future aquatic antifouling strategies: A review,” *Int. J. Mol. Sci.*, vol. 21, no. 14, pp. 1–20, 2020.
- [17] J. M. Hills, J. C. Thomason, and J. Muhl, “A precise and accurate technique for the manufacture of complex three - dimensional surfaces,” *Biofouling*, vol. 13, no. 2, pp. 37–41, 2009.
- [18] T. Sullivan, K. McGuinness, N. E. O’Connor, and F. Regan, “Characterization and anti-settlement aspects of surface micro-structures from *Cancer pagurus*,” *Bioinspiration and Biomimetics*, vol. 9, no. 4, 2014.
- [19] M. Munther *et al.*, “Microfabricated Biomimetic placoid Scale-Inspired surfaces for antifouling applications,” *Appl. Surf. Sci.*, vol. 453, no. September, pp. 166–172, 2018.
- [20] J. P. Maréchal and C. Hellio, “Challenges for the development of new non-toxic antifouling solutions,” *Int. J. Mol. Sci.*, vol. 10, no. 11, pp. 4623–4637, 2009.
- [21] P.-Y. Chen, J. McKittrick, and M. A. Meyers, “Biological materials: Functional adaptations and bioinspired designs,” *J. Mech. Behav. Biomed. Mater.*, vol. 57, no. 1, pp. 1492–1704, 2012.
- [22] W. E. G. Müller *et al.*, “Principles of Biofouling Protection in Marine Sponges : A Model for the Design of Novel Biomimetic and Bio-inspired Coatings in the Marine Environment ?,” pp. 375–398, 2013.
- [23] J. Chapman *et al.*, “Bioinspired synthetic macroalgae : Examples from nature for antifouling applications,” *Int. Biodeterior. Biodegradation*, vol. 86, no. A, pp. 6–13, 2014.
- [24] P. Taylor, V. Caputo, G. Candi, S. Colella, and E. Arneri, “Reproductive biology of turbot (*Psetta maxima*) and brill (*Scophthalmus rhombus*) (Teleostei , Pleuronectiformes) in the Adriatic Sea Reproductive biology of turbot (*Psetta maxima*) and brill (*Scophthalmus rhombus*) (Teleostei , Pleuronectiformes),” no. March 2014, pp. 37–41.
- [25] W. Sweetser, *The Connoisseur’s Guide to Fish & Seafood*. 2009.
- [26] M. V Graham and N. C. Cady, “Nano and Microscale Topographies for the Prevention of Bacterial Surface Fouling,” *Coatings*, vol. 4, no. 1, pp. 37–59, 2014.
- [27] K. Ng, W. Lam, and K. Ng, “2002–2012: 10 Years of Research Progress in Horizontal-Axis Marine Current Turbines,” *Energies*, vol. 6, no. 1, pp. 1497–1526, 2013.

